

SCATTERING AND ABSORPTION

OF SURFACE WAVES BY

ARTHUR'S ISLAND

By: L. S. WIRT

JUNE 1996

SCATTERING AND ABSORPTION

OF SURFACE WAVES BY

ARTHUR'S ISLAND

By: L. S. WIRT

JUNE 1996

ABSTRACT

One of the promising approaches to the extraction of ocean wave energy utilizes a dome shaped artificial atoll to capture incident waves by refraction. The efficiency of such a device will depend on its absorption cross section. A solution to the wave equation is obtained which permits calculation of both scattering and absorption cross sections for an important class of atoll shapes at their design wavelength. A method for approximating the absorption cross section at other wavelengths is also presented.

The dome shape considered is believed to be the optimum shape for ocean wave energy concentration. At the suggestion of John Isaacs, this shape has been designated as "Arthur's Point Island" in honor of R. S. Arthur, his colleague for many years at Scripps Institute. It was Arthur who first explored the refraction around circular atolls by a geometrical optics method.

CONTENTS

<u>Section</u>	<u>Title</u>	<u>Page</u>
	ABSTRACT	i
	CONTENTS	ii
	SYMBOLS	iv
	FIGURES	ix
1.0	INTRODUCTION	1
1.1	Historical Note	1
1.2	Arthur's Point Island	4
2.0	WAVE EQUATION SOLUTIONS, INNER REGION	12
2.1	Arthur's Geometrical Optics Solution	12
2.2	The Potential Function	16
2.3	Modal Impedance	21
2.4	Relation to Arthur's Solution	25
3.0	WAVE EQUATION SOLUTIONS, OUTER REGION	28
3.1	The Potential Function	28
3.2	Differential Scattering	28
3.3	Scattering Cross Section	29
3.4	Absorption Cross Section	29
3.5	Total Cross Section	31
3.6	Comparison of Spheres and Cylinders	31
3.7	Some Predictions	34
4.0	NUMERICAL RESULTS	38
4.1	Cross Sections	38
4.2	Differential Scattering	42

CONTENTS - Continued

<u>Section</u>	<u>Title</u>	<u>Page</u>
5.0	ARTHUR'S ISLANDS WITH CLIPPED SKIRTS	55
5.1	Case 1; Constant r_o , Variable r_c	55
5.2	Case 2; Constant r_c , Variable r_o	57
6.0	RESPONSE OF ARTHUR'S ISLAND TO OFF-DESIGN WAVELENGTHS	64
6.1	The Phantom Island Method	64
6.2	The Shape of Arthur's Island	64
6.3	Best Fit In The Significant Region	65
6.4	Relation of A to B	68
7.0	ABSORPTION CROSS SECTION SPECTRA	71
7.1	The Cross Sections of Phantom Islands	71
7.2	Sample Spectra	71
	REFERENCES	74

SYMBOLS

<u>Symbol</u>	<u>Description</u>
a_m	Arbitrary constant.
A	Radius ratio, $\frac{r_o}{r_o}$
A_m	Complex reflection factor (George).
b_m	Arbitrary constant.
B	Wavelength ratio $\frac{\lambda_o}{\lambda_o}$
c	Celerity.
c_o	Deep water celerity.
c_T	Tangential celerity.
C	Normalized celerity $C = \frac{c}{c_o} \quad C_o = 1$
d	Diameter $d = 2 r_o$
e	Base of natural logarithms.
f	Frequency
f_o	Design frequency.
f'	Off-design frequency.
F	A function of R.
g_m	Mth integration constant.
G	A function of θ .
h	Depth to Arthur's Island.
h'	Depth to a phantom island.
h_o	Depth at perimeter of Arthur's Island.
h_N	Depth at $R = R_N$.
$h_m(\)$	Spherical Hankel function.

SYMBOLS - Continued

<u>Symbol</u>	<u>Description</u>
$h'_m(\)$	Derivative with respect to the argument of a spherical Hankel function.
H_m^1	Hankel function of first kind and order m.
H'_m^1	Derivative of Hankel function with respect to its argument.
i	$\sqrt{-1}$
$j_m(\)$	Spherical Bessel function of first kind and order m.
$j'_m(\)$	Derivative of spherical Bessel function with regard to its argument.
J_m	Cylindrical Bessel function of first kind and order m.
J'_m	Derivative of cylindrical Bessel function with regard to its argument.
k	Wave number.
k_o	Deep water wave number at design wavelength λ_o .
K_o	$k_o r_o$
K'_o	A K_o
m	Order number.
n	Index number.
$n_m(\)$	Spherical Neumann function of order m.
$n'_m(\)$	Derivative of spherical Neumann function with regard to its argument.
N	Number of subdivision of R.
N_m	Cylindrical Neumann function of order m.
N'_m	Derivative of cylindrical Neumann function with regard to its argument.

SYMBOLS - Continued

<u>Symbol</u>	<u>Description</u>
P_m	Amplitude of mth partial wave $p_m = (p_{inc} + p_{scat})_m$
P_{inc}	Amplitude of incident wave.
P_{scat}	Amplitude of scattered wave.
P	Amplitude of plane wave.
P_1, P_2	First and second points in a wave field.
Q_m	Negative of mth component of acoustical admittance.
r	Radial coordinate.
r_o	Limiting radius of Arthur's Island where $c = c_o$.
r_c	Outer radius of clipped Arthur's Island.
r_o	Limiting radius of a phantom island where $c = c_o$.
R	Normalized radius $R = \frac{r}{r_o}$ $R_o = 1$.
R_c	Normalized clipped radius $R_c = \frac{r_c}{r_o}$.
R_N	Nth value of R (outer limit of "significant" region).
R'	Normalized radius of a phantom island $R' = AR$.
R_m	Complex reflection factor (Morse and Ingard).
s	Line segment.
t	Time.
T	Function of time.
T	Wave period (Section 6.4).
u	Natural logarithm of R (a substitute variable).
v	Horizontal particle velocity.
v_m	Horizontal particle velocity in direction of propagation for mth partial wave.
v_{rm}	Radial component of v_m .
$v_{\theta m}$	Tangential component of v_m .

SYMBOLS - Continued

<u>Symbol</u>	<u>Description</u>
x	Coordinate axis.
z	Impedance
z_1, z_2	Characteristic impedance in region 1 and region 2.
z_m	Impedance looking in the direction of propagation for the mth partial wave.
z_{rm}	Impedance looking in the radial direction for the mth partial wave.
$z_{\theta m}$	Impedance looking in the tangential direction for the mth partial wave.
Z_m	z_m normalized by local characteristic impedance $\rho_o c$.
Z_{rm}	z_{rm} normalized by local characteristic impedance $\rho_o c$.
$Z_{\theta m}$	$z_{\theta m}$ normalized by local characteristic impedance $\rho_o c$.
β_m	Acoustical admittance at a boundary ($\beta_m = -Q_m$).
δ_{mn}	Kronecker's delta.
Δ	R.M.S. deviation.
∇	Laplace operator.
ϕ	Angle between ray path and radius.
Φ	Potential function $\Phi = FGT$.
λ	Wavelength.
λ_o	Deep water wavelength at design frequency.
λ'_o	Deep water wavelength at an off design frequency.
ρ_o	Density of water.
$\frac{\partial \sigma}{\partial \theta}$	Differential scattering.
\sum_m	Summation over m.
Σ	Total cross section.

SYMBOLS - Continued

<u>Symbol</u>	<u>Description</u>
Σ_a	Absorption cross section.
Σ_s	Scattering cross section.
θ	Angular coordinate.
θ'	Angular coordinate (Arthur) $\theta' = \theta - \pi$
θ'_0	Initial value of θ' at $R = R_0$.
τ	Reflection coefficient.
ω_0	Design angular frequency.
Ω	$\frac{\omega_0}{m}$
*	Complex conjugate of.

FIGURES

<u>Figure No.</u>	<u>Title</u>	<u>Page</u>
1	SCHEMATIC CROSS SECTION OF "DAM-ATOLL" The dimensions assume a design wave period of about seven seconds.	2
2	DAM-ATOLL SCALE MODEL DYNAMETRIC TESTS IN 1979 The dynamometer is a small D.C. motor which applies a controllable bucking torque to the shaft.	3
3	ARTHUR'S COORDINATE SYSTEM Note that Arthur measured θ' and θ'_0 from the negative x axis.	5
4	C $\text{SIN } \theta'_0$ AS A FUNCTION OF R Any single valued curve in the allowed region represents a physically attainable dome shape.	7
5	C $\text{SIN } \theta'_0$ VS. R FOR ARTHUR'S ISLAND The quantity $\frac{dC}{dR}$ should be regarded as the "slope" of the bottom rather than the geometrical angle of inclination.	9
6	REFRACTION AROUND ARTHUR'S ISLAND AT DESIGN WAVE-LENGTH The rays are shown as terminating in a surf zone, which is the actual case. All rays traverse a logarithmic spiral and the capture appears complete.	13
7	REFRACTION AROUND ARTHUR'S ISLAND FOR A WAVE-LENGTH ONE HALF OF THE DESIGN WAVELENGTH The outer rays escape if the local depth is greater than one half of the incident wavelength. Beyond this depth the incident wave is oblivious of the bottom contour.	14

FIGURES - Continued

<u>Figure No.</u>	<u>Title</u>	<u>Page</u>
8	REFRACTION AROUND ARTHUR'S ISLAND FOR A WAVE-LENGTH TWICE THE DESIGN WAVELENGTH The celerity C is discontinuous at the perimeter. This causes the abrupt change of direction in the outer rays. This is an energy reflective situation.	15
9	GEOMETRY OF THE PRESENT ANALYSIS The radius r is normalized by the outer radius r_0 and the polar angle is measured from the positive x axis. The inner and outer regions are characterized only by the prevailing local normalized celerity C .	17
10	COMPARISON OF RAYS COMPUTED BY ARTHUR AND COMPUTED FROM MODAL IMPEDANCE Each region of the wave front will be best coupled to a particular mode as indicated in the figure.	26
11	THE TRANSPARENCY OF ARTHUR'S ISLAND TO NON-PROPAGATING MODES Arthur's Island exhibits an unexpected transparency to all higher order (non-propagating) modes. Thus they are not reflected.	36
12	SCATTERING CROSS SECTIONS VS. K_0 FOR SOFT, HARD, AND BLACK CYLINDERS AND ARTHUR'S ISLAND Arthur's Island scatters the least due partly to its transparency to higher order modes. The scattering peaks occur at integral values of K_0 .	39
13	ABSORPTION CROSS SECTIONS VS. K_0 FOR THE BLACK BODY AND ARTHUR'S ISLAND The absorptive peaks occur for K_0 a little larger than an integer as each new mode becomes well "cut-on."	40

<u>Figure No.</u>	<u>FIGURES - Continued</u> <u>Title</u>	<u>Page</u>
14	TOTAL CROSS SECTIONS VS. K_o These curves were computed as shown in Table 1 but they may also be obtained by adding Figures 12 and 13.	41
15	DIFFERENTIAL SCATTERING FOR A SMALL HARD CYLINDER $K_o = 1, Q = 0$	43
16	DIFFERENTIAL SCATTERING FOR A LARGE HARD CYLINDER $K_o = 20, Q = 0$	44
17	DIFFERENTIAL SCATTERING FOR A SMALL SOFT CYLINDER $K_o = 1, Q = -\infty$	46
18	DIFFERENTIAL SCATTERING FOR A LARGE SOFT CYLINDER $K_o = 20, Q = -\infty$	47
19	DIFFERENTIAL SCATTERING FOR A SMALL BLACK CYLINDER $K_o = 1, Q = -1$	48
20	DIFFERENTIAL SCATTERING FOR A MEDIUM SIZED BLACK CYLINDER $K_o = 3.6, Q = -1$	49
21	DIFFERENTIAL SCATTERING FOR A LARGE BLACK CYLINDER $K_o = 20, Q = -1$	50
22	DIFFERENTIAL SCATTERING FOR A VERY SMALL ARTHUR'S ISLAND $K_o = 0.9, Q_m = -\sqrt{K_o^2 - m^2}$	51
23	DIFFERENTIAL SCATTERING FOR A SMALL ARHTUR'S ISLAND $K_o = 1, Q_m = -\sqrt{K_o^2 - m^2}$	52
24	DIFFERENTIAL SCATTERING FOR A MEDIUM SIZED ARTHUR'S ISLAND $K_o = 3.6, Q_m = -\sqrt{K_o^2 - m^2}$	53
25	DIFFERENTIAL SCATTERING FOR A LARGE ARTHUR'S ISLAND $K_o = 20, Q_m = -\sqrt{K_o^2 - m^2}$	54

FIGURES - Continued

<u>Figure No.</u>	<u>Title</u>	<u>Page</u>
26	ARTHUR'S ISLANDS WITH CLIPPED SKIRTS Much construction material can be saved by optimum skirt clipping.	56
27	ABSORPTION CROSS SECTION VS. K_o FOR ARTHUR'S ISLAND CLIPPED AT $R_c = .933$ The response curve is shifted to the right by a factor $\frac{1}{R_c}$ but very little change in shape.	59
28	ABSORPTION CROSS SECTION VS. K_o FOR ARTHUR'S ISLAND CLIPPED AT $R_c = 0.8$ The response curve is shifted to the right by a factor $\frac{1}{R_c} = 1.25$ but little change in shape occurs.	60
29	ABSORPTION CROSS SECTION VS. K_o FOR ARTHUR'S ISLAND WITH DRASTIC SKIRT CLIPPING AT $R_c = 0.5$ AND 0.25 The peaks are now sparce due to the shift to the right and the valleys have become very deep.	61
30	CLIPPED ARTHUR'S ISLANDS NORMALIZED TO MAINTAIN CONSTANT DIAMETER The radius r_o may always be chosen to provide a chosen outer radius and desired degree of clipping.	62
31	ABSORPTION CROSS SECTION VS. $K_o R_c$ FOR THE CLIPPED ARTHUR'S ISLANDS OF FIGURE 30 For $R_c \geq 0.8$ the curves are nearly congruent.	63
32	THE RELATION BETWEEN A AND B The points represent A as a function of B that provide the best curve fit between Arthur's Island and a phantom island for two selections of "significant region." The solid curve corresponds to	67

$$A = \sqrt{B}$$

FIGURES - Continued

<u>Figure No.</u>	<u>Title</u>	<u>Page</u>
33	THE SHAPE OF PHANTOM ISLANDS These phantom island shapes are calculated using $A = \sqrt{B}$	70
34	ABSORPTION CROSS SECTION SPECTRA The rolloff for $f'_0/f_0 > 1$ reflects the increasing percentage of escape paths. The undulations for $f'_0/f_0 < 1$ result from mode sparsity for too small an island.	73

NOTE

The name DAM-ATOLL, as used in the captions of Figures 1 and 2, was coined to describe an atoll shaped wave energy extraction device wherein the wave induced flow spills over a top lip.

"DAM-ATOLL" is pronounced in exactly the same way as the mildly profane expletive phrase ('damn-it-all), frequently heard during petroleum shortages.

1.0 INTRODUCTION

1.1 Historical Note

The fact that waves spiral inward around small atolls, and thereby create surf on their lee side, was well known to the most ancient Polynesian navigators, but heavy surf on the lee side was probably an unpleasant surprise to landing parties early in the Pacific campaign of World War II. An investigation of surface wave refraction around circular atolls was undertaken at Scripps Institute of Oceanography by R. S. Arthur. His results were not declassified until 1946.

In 1975 Wirt applied Arthur's analysis to the design of small artificial atolls intended to capture wave energy and convert it to mechanical power. This was accomplished by collecting the surf all around the atoll with guide vanes which directed the inward flow tangentially into a central vertical chamber. The result was a large vortex in the central vessel which served as a "fluid flywheel." Finally the water passed through a turbine wheel before returning to the open sea. The concept is shown schematically in Figure 1.

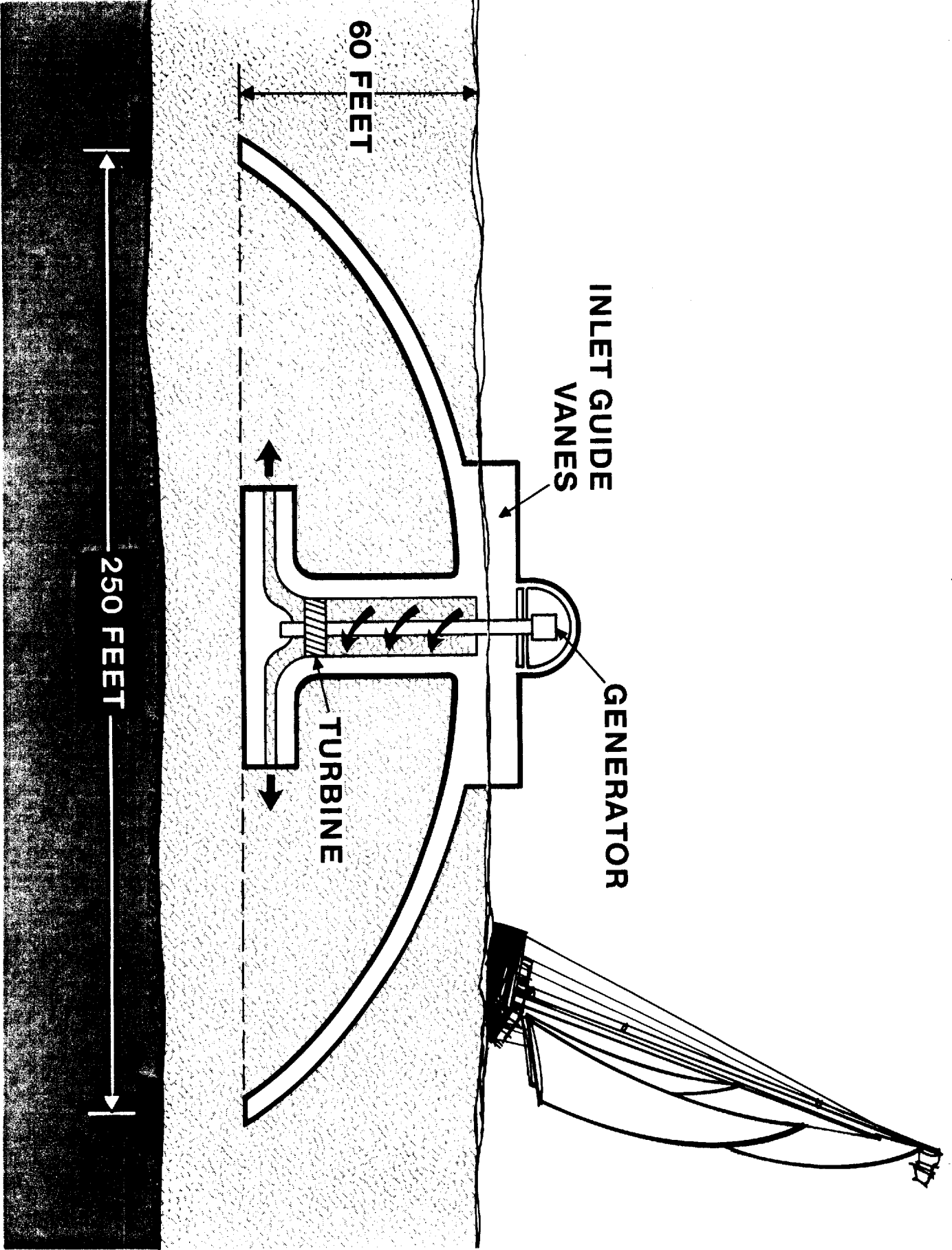
A crude 1/100-scale model was constructed. This model operated in a very lively manner and was extensively tested in 1978-1979. An energy conversion efficiency of about 20% was attained. Figure 2 shows the model being subjected to dynametric tests.

During this era the model was demonstrated to John Isaacs, Robert Wiegel, Michael McCormick and others. Their encouragement provided, for a time, considerable impetus towards optimization of the design, and the concept was patented by Lockheed in twenty-four countries throughout the world, Wirt (1979).

1

SCHEMATIC CROSS SECTION OF "DAM-ATOLL"

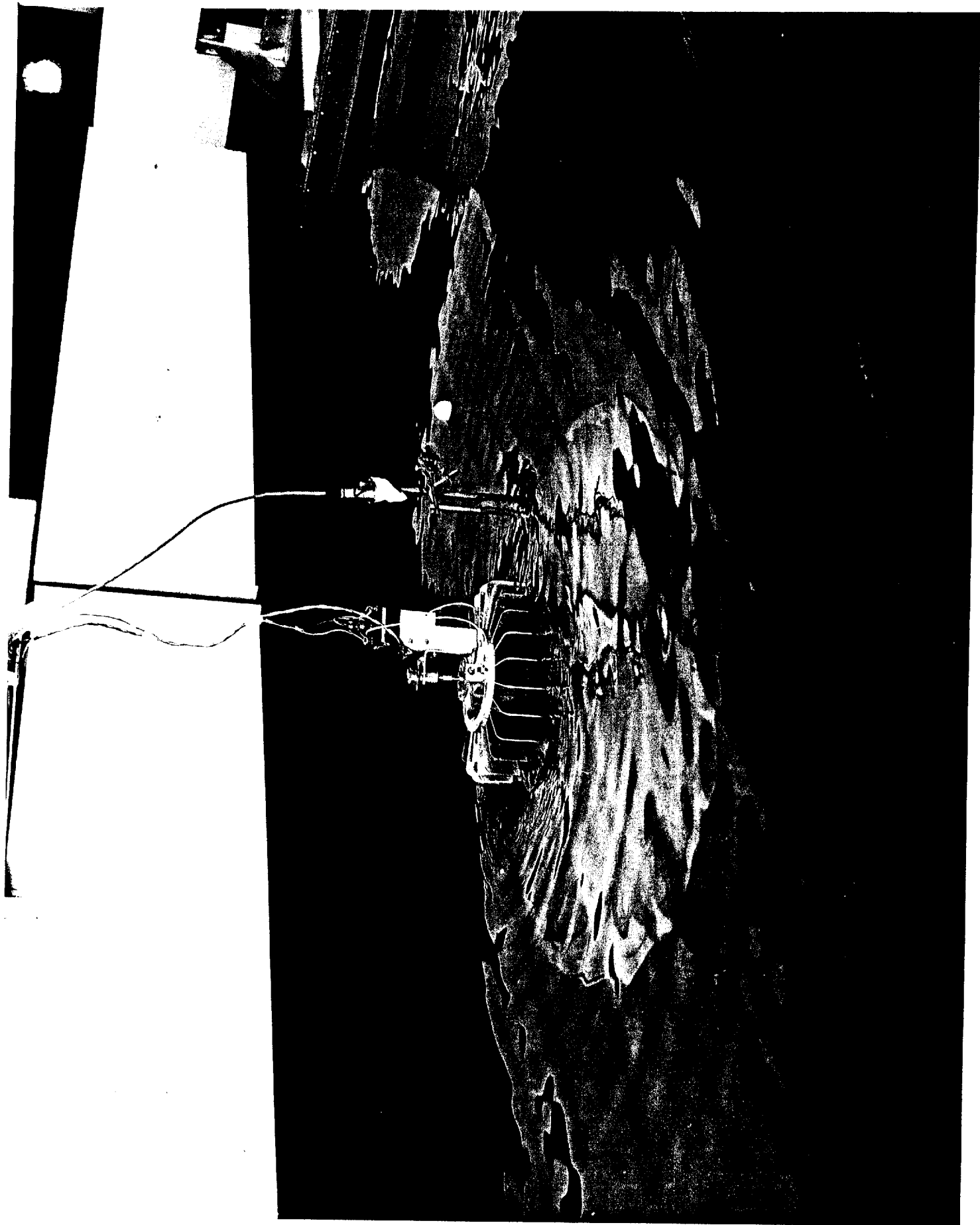
The dimensions assume a design wave period
of about seven seconds.



2

DAM-ATOLL SCALE MODEL DYNAMETRIC TESTS IN 1979

The dynamometer is a small D.C. motor which applies a controllable bucking torque to the shaft.



In 1980, Professor C. C. Mei, of the Massachusetts Institute of Technology pointed out that a scattering analysis of the concept would be very useful to the optimization process. At this point in time, adverse changes in both National and Lockheed Corporate energy policy put the concept into a long hiatus. This paper may help to revive interest in this type of renewable energy source now that patent obstructions are about to expire.

The term, "Arthur's Point Island," as used in this paper was vigorously suggested by John Isaacs. Isaacs was aware of the shape optimization problem and proposed that, once the optimum shape was established, it be designated as "Arthur's Island." The author was happy to adopt this suggestion.

1.2 Arthur's Point Island

Arthur (1946) solved the general problem of wave refraction around islands with circular bottom contours by geometrical optics. His approach was to apply Fermat's principle in the polar coordinate system of Figure 3. The principle states that, given a source point and a receiver point in a medium with position dependent propagation velocity, the ray path will be that which provides the least transit time.

$$t = \int_{P_1}^{P_2} \frac{ds}{c} \quad (\text{minimum}) \quad (1)$$

Application of the calculus of variations led to a solution for plane incident waves.

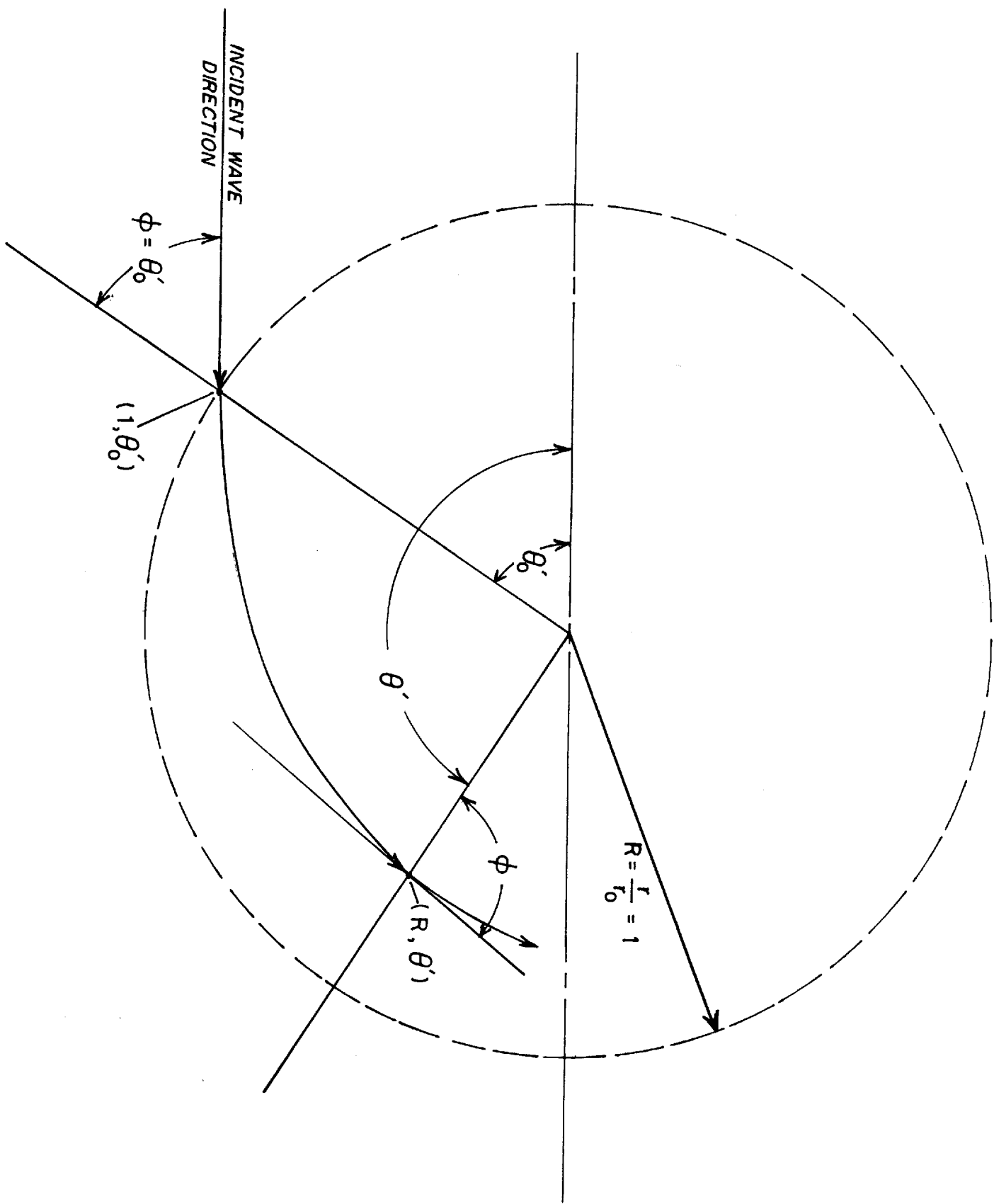
$$\frac{dR}{R \sqrt{\left(\frac{c_o R}{c \sin \theta_o}\right)^2 - 1}} = \pm d\theta' \quad (2)$$

If $\frac{c}{c_o}$ is known as a function of R, equation 2 can always be integrated,

3

ARTHUR'S COORDINATE SYSTEM

Note that Arthur measured θ' and θ'_0 from the negative x axis.



often in closed form but at least numerically, to obtain R as a function of θ' , i.e., the ray path.

Equation 2 may be written

$$\cot \phi = \frac{dR}{Rd\theta'} = \pm \sqrt{\left(\frac{R}{C \sin \theta'_0}\right)^2 - 1} \quad (3)$$

where ϕ is the angle between the ray path and an intersecting radius. This illustrates the dominant role of the square root in determining the ray path. The square root is dominated by the term $\frac{R}{C \sin \theta'_0}$ and its role may be illustrated by plotting $C \sin \theta'_0$ vs. R as is done in Figure 4.

The entire upper left corner of Figure 4 is an "excluded" region for if $\frac{R}{C \sin \theta'_0} < 1$ then $\cot \phi$ is imaginary. These rays veer out again and escape the island.

In the allowed region any single valued locus $C \sin \theta'_0$, R is permissible. An island could be designed to provide the chosen relation between C and R for the ray path incident at θ'_0 at any single deep water wavelength λ_0 because,

$$h = \frac{\lambda_0}{2\pi} C \operatorname{arctanh} C \quad (4)$$

and $h(R)$ defines the physical shape of the atoll.

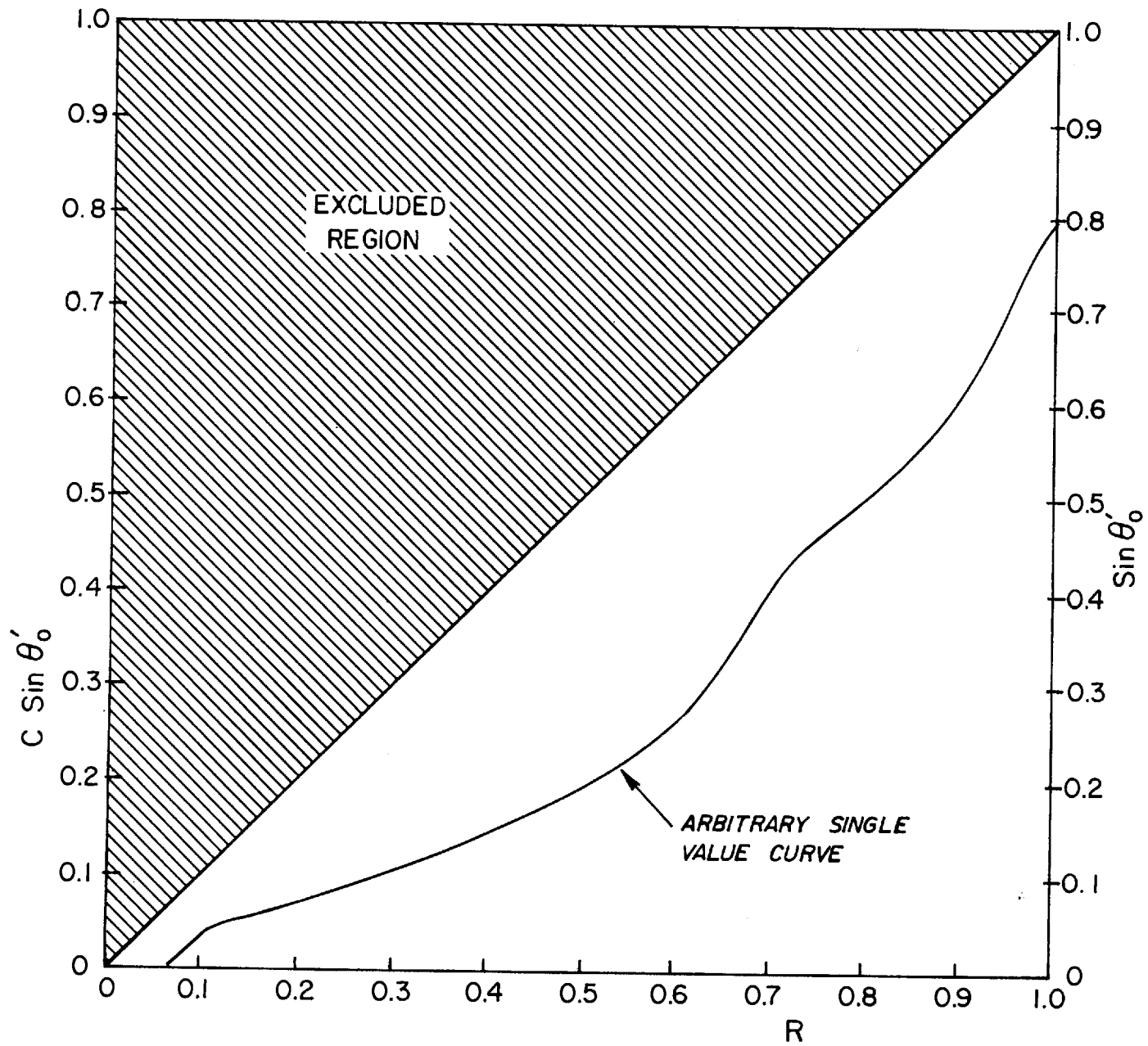
Thus the problem of selecting an optimum dome shape reduces to choosing the relation between the R and C most conducive to energy transmission inward over the atoll and least reflective to the energy at the boundary.

Arthur worked out several special cases in detail. One of these is a "point island" (case 1A) which is defined by the relation $C = R$. This island has a number of noteworthy features. First of all, the angle ϕ

4

$C \sin \theta_0$ AS A FUNCTION OF R

Any single valued curve in the allowed region
represents a physically attainable dome shape.



between any ray path and the successive radii that it crosses remains constant and in fact,

$$\phi = \theta'_0 \quad (5)$$

The ray path is the locus of,

$$R = \exp - (\theta' - \theta'_0) \cot \theta'_0 \quad (6)$$

This is a logarithmic spiral.

Note that the expression

$$\cot \theta'_0 = \sqrt{\frac{1}{\sin^2 \theta'_0} - 1} \quad (7)$$

is a trigonometric identity.

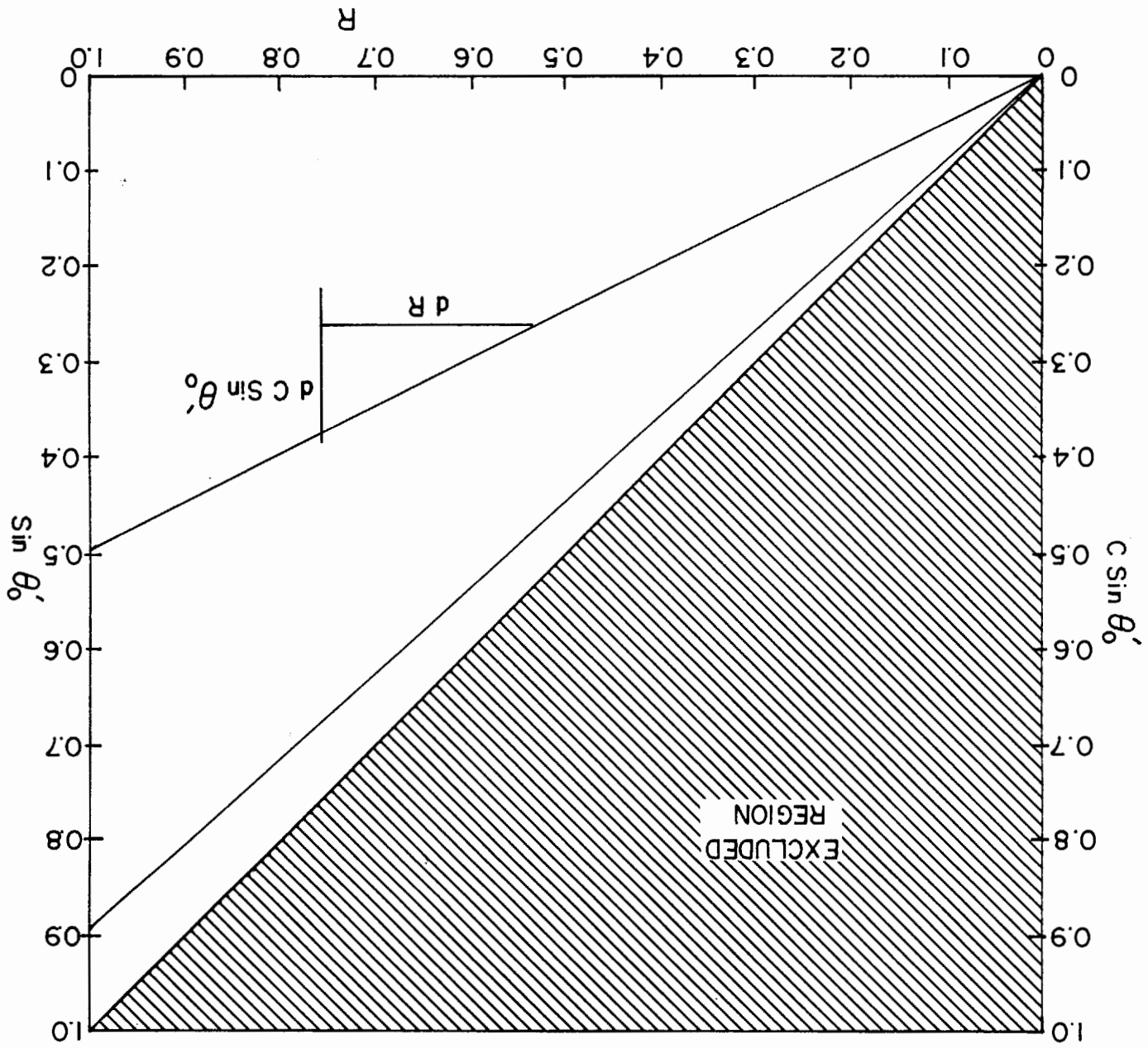
The loci of $C \sin \theta'_0$ vs. R for the point island $R = C$ for various values of θ'_0 are shown in figure 5. For each value of $\sin \theta'_0$, indicated on the right hand vertical scale, the plot is a straight line originating at the origin. The limiting case, $\sin \theta'_0 = 1$, is the boundary of the excluded region. The other limit is $\sin \theta'_0 = 0$ which is the abscissa.

Starting in 1975, when the use of an artificial atoll for wave energy collection was first proposed, the question of what atoll shape would best serve the purpose received considerable attention. It was generally known that "gentle" bottom slopes could transmit wave energy freely whereas "steep" slopes or discontinuities were somewhat reflective. These effects were not quantitatively known except perhaps in shoaling depths. It seems clear however, that what is meant by gentle or steep is not the angle of inclination of the bottom but rather the rate of change of wave celerity that the slope induces. Thus a fairly steep slope in deeper water probably has the same effect on energy flux as some more gentle slope in shallower water so long as $\frac{dC}{dR}$ is the same in both cases. Then to maximize transmission and minimize reflection the contour should minimize the slope $\frac{dC}{dR}$ everywhere (see Figure 5).

5

C SIN θ_0 VS. R FOR ARTHUR'S ISLAND

The quantity $\frac{dC}{dR}$ should be regarded as the "slope" of the bottom rather than the geometrical angle of inclination.



As viewed by acousticians, the problem formulation is very different but the outcome is the same. A propagating surface wave may be assigned a characteristic impedance by forming the ratio of the hydrodynamic pressure to the horizontal component of the particle velocity. The result is

$$z = \rho_0 c \quad (8)$$

where ρ_0 is the (constant) density of the liquid and c is the celerity of the surface wave. This ratio remains constant at any depth since both the pressure and the particle velocity undergo the same exponential decrease with depth. The celerity however is a function of local depth. Thus the characteristic impedance z is a function of local depth.

It follows that any surface wave field may be dealt with as a two dimensional disturbance in a medium of spatially varying characteristic impedance, $\rho_0 c$. Any discontinuity in characteristic impedance is a reflective situation with a reflection coefficient of,

$$\tau = \frac{z_2 - z_1}{z_2 + z_1} \quad (9)$$

For a step from a deep water free field to a shallow water free field this becomes,

$$\tau = \frac{\frac{c}{c_0} - 1}{\frac{c}{c_0} + 1} \quad (10)$$

The step is the limiting case of a celerity gradient. In acoustics, it is axiomatic that minimum reflection and maximum transmission require minimal gradients of characteristic impedance of the medium, i.e., $\frac{dz}{dx}$ minimal.

The foregoing paragraphs presented two of the various lines of reasoning which converge to the conclusion that Arthur's Point Island, (Case 1A) is, in all probability, the most desirable shape for an energy capturing atoll. Although this conclusion has not been quite proven, it is widely accepted. For example, McCormick (1981) identifies the point island with $C = R$ as the optimum shape, without further discussion.

The atoll for which $C = R$ will hereafter be designated as Arthur's Point Island, or simply as Arthur's Island, in accordance with the wish of John Isaacs.

The emergence of Arthur's Point Island as optimum for wave energy capture is a flagrant violation of Murphy's Law, for it is, by far, the most tractable mathematically. In geometrical optics analysis, only if R is proportional to C does the square root of equation 2 become a constant so that the integration is trivial. In the scattering analysis which follows, it will be shown that, if $R = C$, then Bessels Equation will collapse into an elemental differential equation, solvable by inspection in terms of elemental functions. *

It is to be clearly understood that Arthur's Point Island was selected as optimum because of its physical merits and was then found to be mathematically tractable. Any allegation that it was declared optimum because it is tractable, is vigorously denied.

*The author recommends "inspecting" compilations of solved differential equations, e.g., Dwight, H. B., 1961, Tables of Integrals and Other Mathematical Data, Macmillan, N.Y.

2.0 WAVE EQUATION SOLUTIONS, INNER REGION

2.1 Arthur's Geometrical Optics Solution

In a very real sense, Arthur solved the wave equation for the surface area above any dome-like structure. He provided a general method for tracing the ray paths from the outer perimeter to zero depth for infinitesimal waves or to breaking depth for small finite waves. Local wave energy concentrations may be deduced from the lateral spacing of the ray paths.

Figure 6 presents the ray paths for Arthur's Point Island for wavelength λ_0 , where λ_0 is the design wavelength of the dome shape. Note that the capture of incident waves appears total. Figure 7 presents the ray paths for shorter waves ($\lambda'_0 = 0.5 \lambda_0$) incident upon the same dome shape. Now the outer rays escape outside of the depth for which $h = 0.5 \lambda'_0$. Figure 8 presents the ray paths generated by waves with wavelength $\lambda'_0 = 2.0 \lambda_0$, again incident on the original dome. The capture appears total but the ray path is discontinuous across the outer boundary due to the abrupt change in refractive index at the perimeter. This is an intrinsically reflective situation.

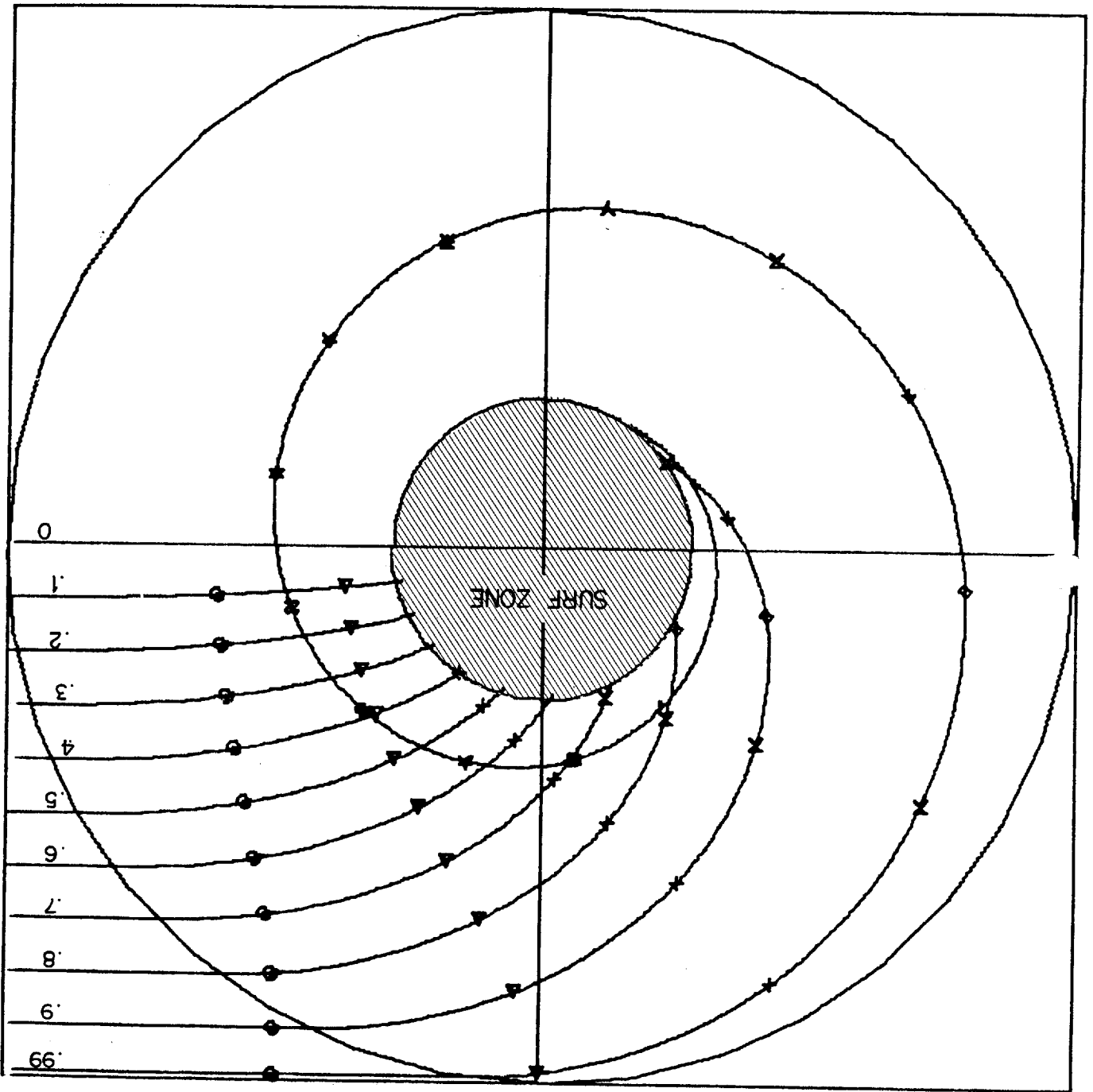
To illustrate this, Arthur's analysis is general enough to apply to an obstacle comprising a simple solid cylinder submerged a little beneath the surface. Now all refraction occurs at the perimeter in a discontinuous manner and the straight ray paths inside can be constructed (approximately) by applying Snell's law. The degree of convergence appears attractive but it is obvious that the reflection at the boundary must be large.

Referring again to Figure 6, one peculiarity of Arthur's solution is that this display of ray paths applies equally well to all diameters of atoll. r_0 may be assigned any value large or small. In his cylindrical coordinates, θ' is "ordinary," r is normalized by (any) r_0 , h and λ_0 do not appear at all except in the calculation of the local depth necessary to provide the desired relationship between C and R . It taxes credulity to think that a

6

REFRACTION AROUND ARTHUR'S ISLAND AT DESIGN WAVE-
LENGTH

The rays are shown as terminating in a surf zone, which is the actual case. All rays traverse a logarithmic spiral and the capture appears complete.

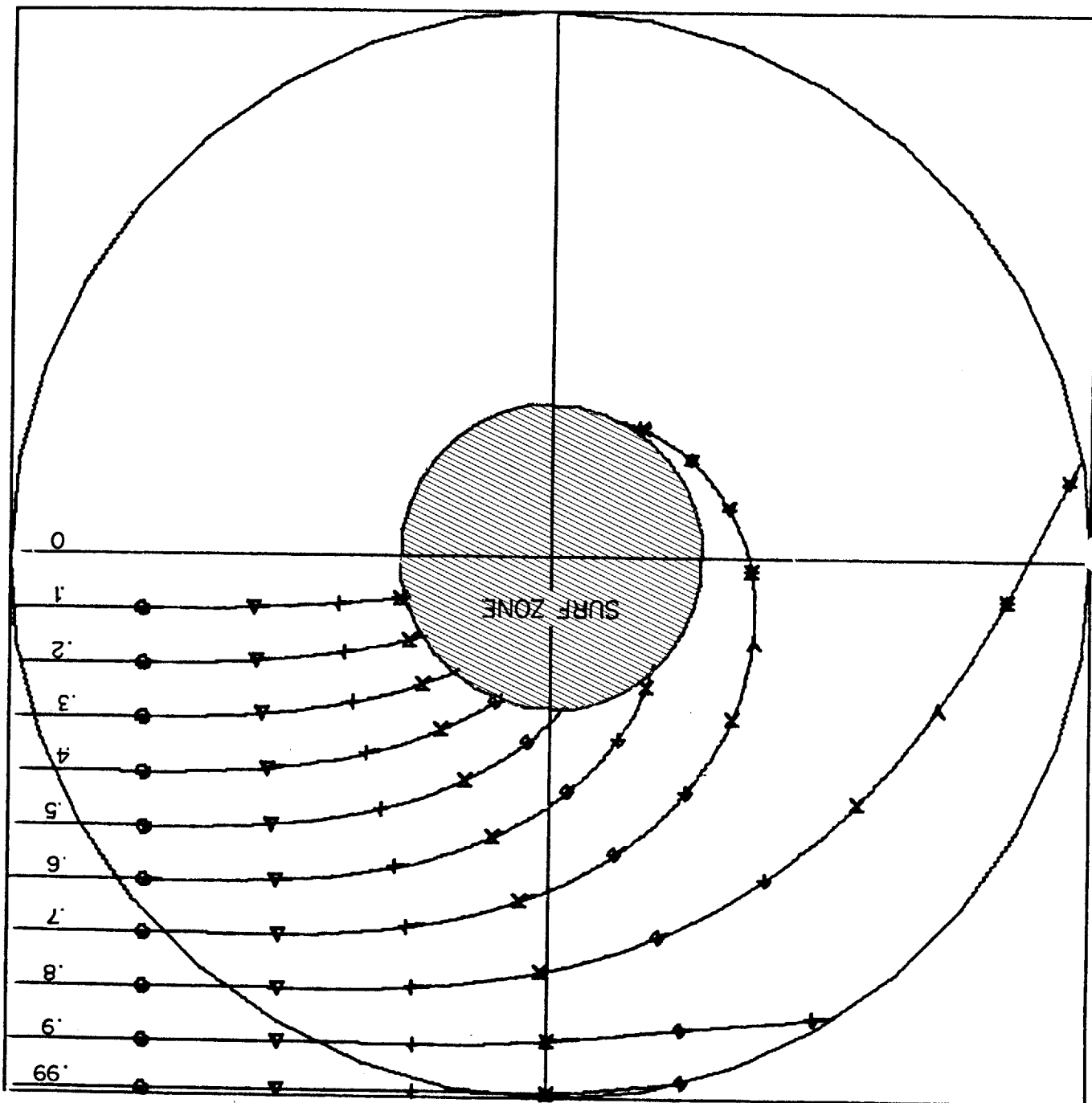


7

REFRACTION AROUND ARTHUR'S ISLAND FOR A WAVE-
LENGTH ONE HALF OF THE DESIGN WAVELENGTH

The outer rays escape if the local depth is
greater than one half of the incident wave-
length. Beyond this depth the incident wave
is oblivious of the bottom contour.

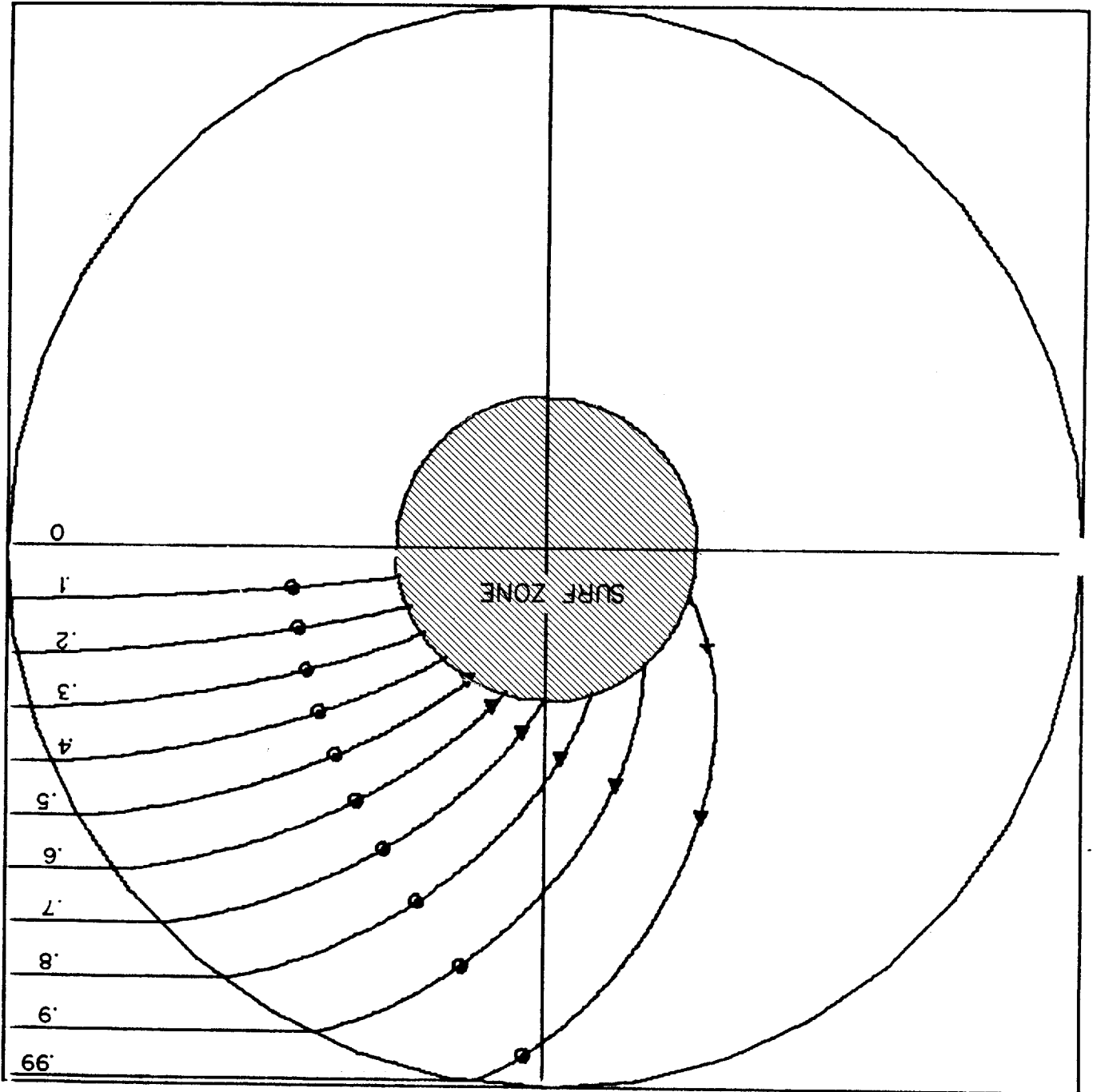




8

REFRACTION AROUND ARTHUR'S ISLAND FOR A WAVE-
LENGTH TWICE THE DESIGN WAVELENGTH

The celerity C is discontinuous at the perimeter. This causes the abrupt change of direction in the outer rays. This is an energy reflective situation.



very small Arthur's Island and a very large one could behave the same. Thus the geometrical optics analysis provides no help in actually sizing a wave collecting atoll or predicting its energy absorption capabilities. Professor C. C. Mei in 1980 pointed out the need for a scattering and absorption analysis to cope with this problem. The writer approached this task with considerable trepidation.

2.2 The Potential Function

The polar coordinates to be used are shown in Figure 9. Plane, linear, monochromatic waves propagate in the positive x direction. These coordinates differ from those of Arthur in that θ is now measured from the positive x axis. A circular boundary at $r = r_0$ divides the plane into an inner region $r \leq r_0$ and an outer region $r > r_0$. For the outer region, $c = c_0$, the deep water celerity, whereas, in the inner region, the celerity is some function of r .

The linear wave equation applies to both regions.

$$\nabla^2 \phi = \frac{1}{c^2} \frac{\partial^2 \phi}{\partial t^2} \quad (11)$$

In polar coordinates,

$$\frac{\partial^2 \phi}{\partial r^2} + \frac{1}{r} \frac{\partial \phi}{\partial r} + \frac{1}{r^2} \frac{\partial^2 \phi}{\partial \theta^2} = \frac{1}{c^2} \frac{\partial^2 \phi}{\partial t^2} \quad (12)$$

At this point it is convenient to introduce Arthur's normalized radius R and celerity C

$$R = \frac{r}{r_0} \quad (R_0 = 1) \quad (13)$$

$$C = \frac{c}{c_0} \quad (C_0 = 1) \quad (14)$$

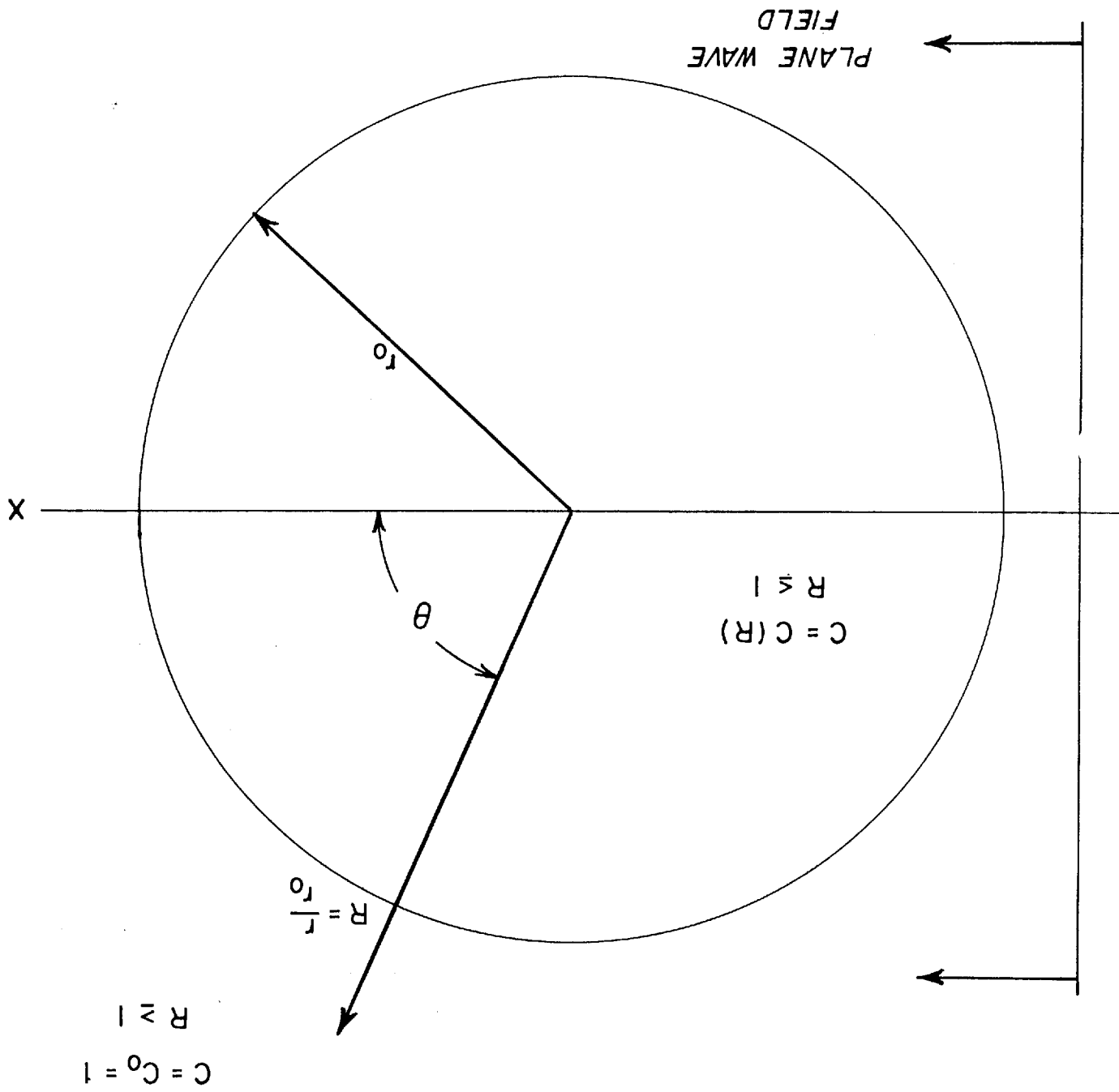
We choose the time dependence of ϕ to be a factor T

$$T = \exp - i \omega_0 t \quad (15)$$

9

GEOMETRY OF THE PRESENT ANALYSIS

The radius r is normalized by the outer radius r_0 and the polar angle is measured from the positive x axis. The inner and outer regions are characterized only by the prevailing local normalized celerity C .



also introduce,

$$K_o = k_o r_o \quad (16)$$

where k_o is the deep water wave number

$$k_o = \frac{\omega_o}{c_o} \quad (17)$$

Then

$$R^2 \frac{\partial^2 \phi}{\partial R^2} + R \frac{\partial \phi}{\partial R} + \frac{K_o^2}{C^2} R^2 \phi + \frac{\partial^2 \phi}{\partial \theta^2} = 0 \quad (18)$$

The variables may be separated by setting

$$\phi = F(R) G(\theta) T(t) \quad (19)$$

and dividing through by ϕ to obtain

$$\frac{R^2}{F} \frac{d^2 F}{dR^2} + \frac{R}{F} \frac{dF}{dR} + \frac{K_o^2}{C^2} R^2 + \frac{1}{G} \frac{d^2 G}{d\theta^2} = 0 \quad (20)$$

This is identically true if,

$$R^2 \frac{d^2 F}{dR^2} + R \frac{dF}{dR} + \frac{K_o^2}{C^2} R^2 F - m^2 F = 0 \quad (21)$$

and

$$\frac{d^2 G}{d\theta^2} = -m^2 G \quad (22)$$

It is clear that G is harmonic in θ and a distinct solution exists for each value of m which is allowed by the boundary conditions. By requiring continuity in the θ direction, m is restricted to positive or negative integers or zero. Each represents a separate and distinct allowed mode. G is then any allowed G_m for $m = -\infty$ to $m = \infty$; where,

$$G_m = g_m e^{im\theta} \quad (23)$$

and g_m is allowed to be complex.

The need for symmetry about the x axis requires that each ϕ_m be an even function. As a result of this boundary condition, $g_{-m} = g_m$.

It is now important to emphasize that $g_m \exp im\theta$ and $g_m \exp -im\theta$ are two separate and distinct modes which are equal in magnitude but when multiplied by $T = \exp -i \omega_0 t$ become counter rotating to form the standing wave pattern most commonly written $\cos m\theta$. To consider modal impedance the modes must be kept separate.

After modal impedances have been calculated the exponentials may be combined in pairs into

$$G_m = g_m \cos m\theta \quad (24)$$

in the more usual way.

The equation for F may be written,

$$R^2 \frac{d^2 F}{dR^2} + R \frac{dF}{dR} + K_o^2 \frac{R^2}{C^2} F - m^2 F = 0 \quad (25)$$

which is a standard form for Bessel's equation. Its solution is very different for the inner and outer regions and these will be considered separately.

For the particular case designated as Arthur's Island, $C = R$. As a result of this substitution Bessel's equation collapses to,

$$R^2 \frac{d^2 F}{dR^2} + R \frac{dF}{dR} + (K_o^2 - m^2) F = 0 \quad (26)$$

This reduces to a linear equation by a change of variable, e.g., see Dwight (1961).

$$\text{Set } R = \exp u \quad (27)$$

$$\frac{d^2 F}{du^2} + (K_o^2 - m^2) F = 0 \quad (28)$$

Thus F is any of an infinite number of solutions,

$$F_m = a_m \exp i \sqrt{(K_o^2 - m^2)} \ln R + b_m \exp - i \sqrt{(K_o^2 - m^2)} \ln R \quad (29)$$

So long as $K_o > m$, the square root is real and F_m represents propagating waves. Since $T = \exp - i \omega_o t$, the first term of F_m represents outward propagation and the second term inward propagation.

It can be shown that the radially inward velocity of propagation decreases rapidly enough that the transit time from $R = 1$ to $R = 0$ is infinite. Thus the point $R = 0$ is an "infinite termination." There can be no reflected wave, so $a_m = 0$.

$$F_m = b_m \exp - i \sqrt{K_o^2 - m^2} \ln R \quad (30)$$

The situation is reminiscent of Zeno's Paradox which states fallaciously that an arrow can never strike its target. This is because it must first traverse half the distance to the target, then half the remaining distance, etc., ad infinitum.

If however, the statement is modified to require that at each halving of the distance the velocity is also cut in half, then all finite increments of time are equal and infinite in number. Indeed the arrow will never reach its target. Similarly if $R = C$ by definition, then the wave can never arrive at $R = 0$ and is constrained to its logarithmic spiral forever.

This argument should be satisfactory to a mathematician. It is less likely to satisfy engineers, at least as it applies to wave concentration devices. For them, it is pointed out that in the actual application to the wave energy capture device, the real wave breaks at some point, typically at $R = .3$ or $.4$. The resulting bore is guided into a very efficient energy sink such that even the roll back of water is negligible. This energy and fluid sink assures negligible reflection.

Thus for the entire inner region over any Arthur's Island

$$\Phi = \sum_{m=-\infty}^{\infty} b_m g_m \exp -i \sqrt{K_o^2 - m^2} \ln R \times \exp i m \theta \times \exp -i \omega_o t \quad (31)$$

This solution for the inner region $R < 1$ bears a striking resemblance to the "Spinning Modes" of Tyler and Sofrin (1961). The wave pattern over Arthur's Island is comprised of paired, counterrotating, sinusoidal m lobed patterns. There is an abrupt cut off of the modes. For all $m > K_o$ the square root is purely imaginary.

$$\sqrt{K_o^2 - m^2} = i \sqrt{m^2 - K_o^2} \quad (32)$$

In the inner region $\ln R$ is always negative and increases in absolute value as R decreases. Thus the non-harmonic wave amplitude decreases very rapidly towards the center. All of the higher order modes are non-propagating and exhibit an exponentially decaying amplitude radially inward, i.e., are cutoff.

For the first few modes $m < K_o$ so $\sqrt{K_o^2 - m^2}$ is real.

This represents a harmonic propagating wave moving radially inward with decreasing velocity. Note that the $m = 0$ mode always propagates. Fortunately for the purpose of wave energy concentration, most of the energy in an incident plane wave resides in the first few modes.

2.3 Modal Impedance

In acoustics a common approach to scattering problems is to assign a local or "point" impedance to the surface of the circle $R = 1$. Often this surface point impedance is assumed to be independent of mode number.

If, as is true in the case being considered, wave propagation occurs within the boundary, the surface impedance is called a distributed impedance and is not independent of mode number. If the modal impedances can be determined,

then very convenient solution methods, e.g., George (1979) become available. An exploration of modal impedance also provides additional insight into the nature of the wave field over Arthur's Island.

For each distinct mode the following relations apply (the + mth mode is distinct from the -mth mode), Skudrzyk (1971).

Radial particle velocity

$$v_{rm} = -\frac{\partial \phi_m}{\partial r} = +i \sqrt{(K_o^2 - m^2)} \frac{1}{r} \phi_m \quad (33)$$

Tangential particle velocity

$$v_{\theta m} = -\frac{1}{r} \frac{\partial \phi_m}{\partial \theta} = \frac{-im}{r} \phi_m \quad (34)$$

Total particle velocity in the direction of propagation, v_m

$$v_m^2 = v_{rm}^2 + v_{\theta m}^2 \quad (35)$$

$$v_m^2 = -\frac{(K_o^2 - m^2)}{r^2} \phi_m^2 - \frac{m^2}{r^2} \phi_m^2 \quad (36)$$

$$v_m^2 = -\frac{K_o^2}{r^2} \phi_m^2 \quad (37)$$

$$v_m = \frac{+i}{r} K_o \phi \quad (38)$$

Pressure

$$p = \rho_o \frac{\partial \phi_m}{\partial t} = -i \omega_o \rho_o \phi_m \quad (39)$$

and thus the various modal impedances are

$$z_{rm} = \frac{-K_o}{\sqrt{(K_o^2 - m^2)}} \rho_o c \quad (40)$$

$$z_{\theta m} = \frac{-i \omega_o r}{-im} \rho_o = \frac{K_o}{m} \rho_o c \quad (41)$$

$$z_m = \pm \rho_o c \quad \text{for all } m \quad (42)$$

These may be normalized by the local characteristic impedance $\rho_o c$.

$$Z_{rm} = \frac{-1}{\sqrt{1 - \frac{m^2}{K_o^2}}} \quad (43)$$

$$Z_{\theta m} = \frac{K_o}{m} \quad (44)$$

$$Z_m = \pm 1 \quad \text{for all } m \quad (45)$$

Note that,

$$Z_{rm} = \frac{-1}{\sqrt{1 - \frac{1}{Z_{rm}^2}}} \quad (46)$$

All three modal impedances warrant careful consideration. Z_{rm} provides the boundary condition for each mode necessary to use the impedance type of scattering analysis such as that set forth by George (1979). The coordinate system used by George, and used in this paper, considers the radius as positive in the outward direction.

The acoustical impedance of a surface is commonly taken to be that looking into the surface. Therefore the acoustical modal impedance at the perimeter of Arthur's Island is,

$$\text{acoustical } z_{rm} = \frac{K_o}{\sqrt{K_o^2 - m^2}} \rho_o c \quad (47)$$

or

$$\text{acoustical } Z_{rm} = \frac{K_o}{\sqrt{K_o^2 - m^2}} \quad (48)$$

This radial impedance looking into the perimeter of Arthur's Island is real for the first few modes for which $m < K_o$. As a result, energy may cross the boundary. For the rest of the modes, $m > K_o$, the impedance becomes purely imaginary and no energy will cross the boundary. The behavior of these higher order modes bounded by the imaginary Z_{rm} will be discussed in detail later. It will be shown then that they are not reflected.

The tangential impedance $Z_{\theta m}$ is always real. This is consistent with the view that the individual circumferential modes are rotating in lobed patterns which occur in counter rotating pairs to form m lobed standing wave patterns. Because the waves are monochromatic with angular frequency ω_o , the angular velocity of rotation is $\Omega = \frac{\omega_o}{m}$. The tangential phase velocity at radius r_o is,

$$c_T = \frac{\omega_o r_o}{m} = \frac{K_o}{m} c \quad (49)$$

The tangential impedance at any radius r is

$$\rho_o c_T = \frac{K_o}{m} \rho_o c \quad (50)$$

So long as $m < K_o$ the modes are "fast," since at the perimeter, $\frac{K_o}{m} c_o > c_o$.

The corresponding radial modes are "cut-on" and propagate inward. If $m > K_o$ then the modes are "slow" and the radial modes are "cut-off." They now exhibit a nonharmonic nature and an exponential type of amplitude decay. Note that the peripheral phase velocity of the zero order mode is infinite so it is always "cut-on."

The wave impedance looking in the direction of propagation is always $\rho_0 c$ for any propagating mode at any point over the island. This is exactly the characteristic impedance at that point. Thus a perfect impedance match exists over Arthur's Island for all propagating modes.

2.4 Relation to Arthur's Solution

With the aid of the modal impedance calculations above it is possible to make an instructive comparison between the present analysis and some results of Arthur's optical approach.

Arthur (1946), case 1A, showed that a plane wave incident on the boundary at any point θ'_0, R_0 , ($\theta + \pi, R_0$ in the present rotation) the ray continues on a logarithmic spiral. The initial angle between the ray path and the radius at the perimeter is θ'_0 . This angle remains constant at all successive crossings of radii.

From the modal analysis it is evident that the angle between the direction of propagation and any radius is a constant ϕ . Clearly,

$$\theta'_0 = \phi \quad (51)$$

For Arthur's Island,

$$\cot \theta'_0 = \frac{dR}{Rd\theta} = -\sqrt{\frac{1}{\sin^2 \theta'_0} - 1} \quad (52)$$

From the modal analysis results

$$\cot \phi = \frac{v_{rm}}{v_{\theta m}} = -\sqrt{\frac{K_0^2}{m^2} - 1} \quad (53)$$

$$\theta'_0 = \arcsin \frac{m}{K_0} \quad (54)$$

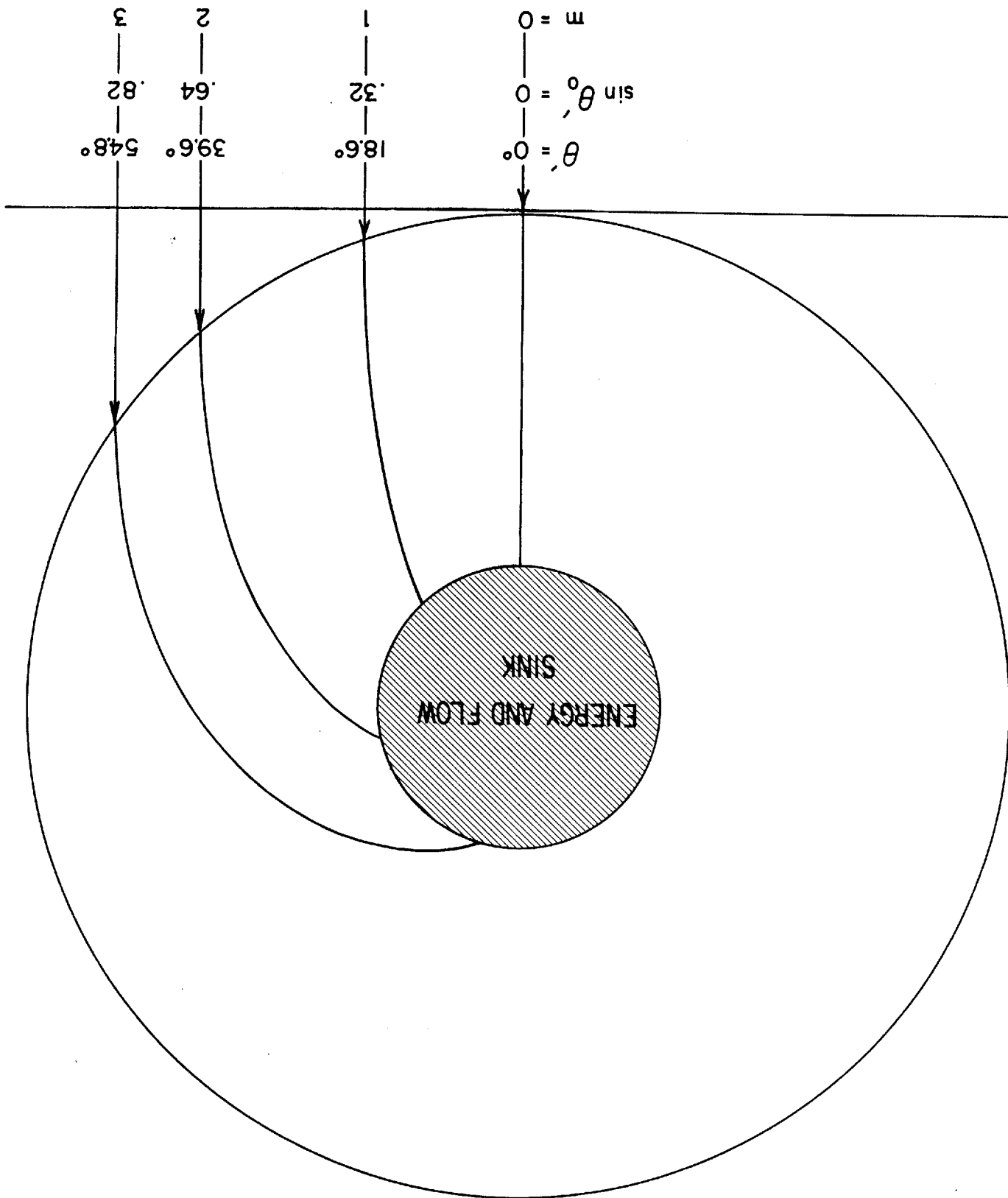
Figure 10 shows the case of Arthur's Island for which

$$K_0 = \frac{\pi d}{\lambda_0} = \pi \quad (55)$$

10

COMPARISON OF RAYS COMPUTED BY ARTHUR AND COMPUTED
FROM MODAL IMPEDANCE

Each region of the wave front will be best coupled
to a particular mode as indicated in the figure.



Note that the incident vectors are rather evenly spaced. Each local region of wave front would predominantly drive the m lobed mode as marked. Each ray path shown sees the impedance $\rho_0 c_0$ at the perimeter and continues to see the local characteristics impedance $\rho_0 c$ over its entire logarithmic spiral trajectory towards $R = 0$ (which in theory it never reaches).

3.0 WAVE EQUATION SOLUTIONS, OUTER REGION

3.1 The Potential Function

For the outer region, $R > 1$, the normalized celerity $C = C_o = 1$ everywhere. As a result, equation 21 becomes,

$$\frac{d^2 F}{dR^2} + \frac{1}{R} \frac{dF}{dR} + \left(K_o^2 - \frac{m^2}{R^2} \right) F = 0 \quad (56)$$

which is Bessel's equation in standard form. F_m is any Bessel Function. G as presented in equation 23, and T in equation 15 remain the same and ϕ may still be written,

$$\phi = \sum_{m=-\infty}^{\infty} F_m G_m T \quad (57)$$

3.2 Differential Scattering

George (1979) provides a convenient formulation for the differential scattering of a circle of finite impedance as follows,

$$P_{inc} = P e^{-i \omega_o t} \sum_{m=0}^{\infty} i^m (2 - \delta_{m0}) J_m(kr) \cos m \theta \quad (58)$$

$$P_{scat} = P e^{-i \omega_o t} \sum_{m=0}^{\infty} i^m (2 - \delta_{m0}) A_m H_m^1(kr) \cos m \theta \quad (59)$$

$$A_m = - \frac{J_m'(k r_o) - i Q_m J_m(k r_o)}{H_m^1(k r_o) - i Q_m H_m^1(k r_o)} \quad (60)$$

The differential scattering is then

$$\frac{\partial \sigma}{\partial \theta} = \frac{2}{\pi k} \left| \sum_{m=0}^{\infty} (2 - \delta_{m0}) A_m \cos m \theta \right|^2 \quad (61)$$

The quantity Q_m is the negative of the normalized acoustical admittance β_m , because of his choice of positive outward normal.

3.3 Scattering Cross Section

The scattering cross section is

$$\sum_S = \int_0^{2\pi} \frac{\partial \sigma}{\partial \theta} d\theta \quad (62)$$

$$\sum_S = \int_0^{2\pi} \frac{2}{\pi k} \left| \sum_{m=0}^{\infty} (2 - \delta_{m0}) A_m \cos m \theta \right|^2 d\theta \quad (63)$$

After some manipulation this becomes,

$$\sum_S = \frac{2}{k} \sum_{m=0}^{\infty} (2 - \delta_{m0})^2 \left| A_m \right|^2 \quad (64)$$

It is more convenient to plot cross sections normalized by r_0 , i.e.,

$$\frac{1}{r_0} \sum_S \text{ vs. } k r_0$$

3.4 Absorption Cross Section

Considerably more effort is required to obtain the corresponding expression for absorption cross section.

The energy absorbed from each component wave at any point on the perimeter is the inward energy flux. The m th component energy absorbed from the m th component wave is the integral of the m th component inward energy flux around the perimeter. The total energy absorbed is then the summation of these partial energy absorptions over the propagating modes.

The m th component of energy flux is, $\text{Re } p_m v_m^*$

where

$$p_m = p_{inc} + p_{scat} \text{ for the } m\text{th component wave}$$

$$v_{mr} = \text{radial component of } v_m$$

$$v_m = v_{inc} + v_{scat} \text{ for the } m\text{th component wave}$$

Then

$$v_{mr} = \beta_m p_m = p_m (-Q_m) \quad (65)$$

$$v_{mr}^* = p_m^* (-Q_m)^* \quad (66)$$

Then

$$\text{Re } p_m v_{mr}^* = |p_m|^2 \text{Re } (-Q) \quad (67)$$

So

$$\sum_a = \sum_{m=0}^{\infty} \int_0^{2\pi} |p_m|^2 \text{Re } (-Q) d\theta \quad (68)$$

By rearrangement, equation 60 becomes,

$$-Q_m = \frac{i(J_m(k r_o) + A_m H_m^{1'}(k r_o))}{(J_m(k r_o) + A_m H_m^1(k r_o))} \times \frac{\left((J_m(k r_o) + A_m H_m^1(k r_o))^*\right)^*}{\left((J_m(k r_o) + A_m H_m^1(k r_o))^*\right)^*} \quad (69)$$

The numerator may be fully expanded and cross multiplied which leads to 25 terms, twelve of which are real. The real terms collect into

$$\left((J_m'(k r_o) N_m(k r_o) - J_m(k r_o) N_m'(k r_o)) \left(|A_m|^2 + \text{Re } A_m \right) \right) \quad (70)$$

The demoninator of equation 69 is clearly

$$\frac{|p_m|^2}{(2 - \delta_{m0})^2 \cos^2 m\theta} \quad (71)$$

By identity,

$$(J'_m(k r_o) N_m(k r_o) - J_m(k r_o) N'_m(k r_o)) = \pm \frac{2}{\pi k r_o} \quad (72)$$

See Abramowitz (1964) items 9.1.32 and 9.1.34.

The sign ambiguity may be resolved with the aid of Abramowitz (1964) item 9.1. . The negative sign proves to be the proper choice for this problem. These results assemble to,

$$\left| p_m \right|^2 \operatorname{Re}(-Q) = (-1) (2 - \sigma_{m0})^2 \frac{2}{\pi k r_o} \cos^2 m\theta (|A_m|^2 + \operatorname{Re} A_m) \quad (73)$$

and the term by term integration from 0 to 2π yields

$$(-1) (2 - \sigma_{m0})^2 \frac{2}{k r_o} (|A_m|^2 + \operatorname{Re} A_m) \quad (74)$$

Thus

$$\sum_a = \frac{2}{k} \sum_{m=0}^{\infty} (2 - \sigma_{m0})^2 (-1) (|A_m|^2 + \operatorname{Re} A_m) \quad (75)$$

3.5 Total Cross Section

The sum of the scattering and absorption cross sections is called the total cross section. Total cross section is a measure of the overall disturbance of the incident wave by an object, and is zero for a transparent body. An expression for total cross section may be obtained by the direct addition of equations 64 and 75.

$$\begin{aligned} \Sigma &= \Sigma_s + \Sigma_a \\ &= \frac{2}{k} \sum_{m=0}^{\infty} (2 - \sigma_{m0})^2 (-\operatorname{Re} A_m) \end{aligned} \quad (76)$$

3.6 Comparison of Spheres and Cylinders

The methods used in the preceding sections closely parallel those used by Morse and Ingard (1968) for the absorptive sphere. It is then not sur-

prising that the results are so similar that the expressions for spherical cross sections may be transposed into the cylindrical case in a very simple way.

Table 1 presents Morse and Ingard's cross sections for spheres and the present expressions for cylinders. The table also projects Morse and Ingard notation to the case of cylinders and applies George's notation to the case of spheres.

In making these comparisons it is to be understood that:

- o All Bessel functions used in the spherical cases are spherical Bessel functions.
- o All Bessel functions used in the cylindrical cases are cylindrical Bessel functions.

Thus after Morse and Ingard:

$$(1 + R_m) = 2 \frac{j'_m(k r_o) + i \beta_m j_m(k r_o)}{h'_m(k r_o) + i \beta_m h_m(k r_o)} \quad (77)$$

$$(\beta = -Q)$$

and after George

$$A_m = - \frac{J'_m(k r_o) - i Q J_m(k r_o)}{H_m^{-1}(k r_o) - i Q H_m^{-1}(k r_o)} \quad (78)$$

$$1 + R_m \sim -2A$$

Note that Morse and Ingard invoke the spherical Bessel function identity

$$j'_m(k r_o) h_m(k r_o) - j_m(k r_o) h'_m(k r_o) = - \frac{i}{k^2 r_o^2} \quad (79)$$

which may be written

$$j'_m(k r_o) n_m(k r_o) - j_m(k r_o) n'_m(k r_o) = - \frac{1}{k^2 r_o^2} \quad (80)$$

The cylindrical identity already cited is

$$J'_m(k r_o) N_m(k r_o) - J_m(k r_o) N'_m(k r_o) = -\frac{2}{\pi k r_o} \quad (81)$$

The difference in the right hand sides provides the difference in the initial factors for the spherical and cylindrical cross sections.

The factors

$$(2m + 1) \sim (2 - \delta_{m0})$$

arise from the use of spherical and polar coordinates. The existence of these parallels reenforced confidence in equations 64, 75, and 76.

The expressions for cylinders in Table 1 for the scattering, absorption, and total cross sections may be used for Arthur's Island and for more familiar cases which provide a frame of reference and a check on the over-all method. For example, if all $Q_m = 0$, this is the rigid body. If all $Q_m = -\infty$, this is the soft body case (pressure release surface). Setting all $Q_m = -1$ represents the perfectly absorptive case, the black body.

Another interesting special case is that of the transparent body which neither scatters nor absorbs. It is clear from equations 64 and 75 that this can occur if all A_m vanish. Setting equation 60 to zero and solving for Q_m gives,

$$Q_m = -i \frac{J'_m(K_o)}{J_m(K_o)} \quad (82)$$

So long as Q_m is purely imaginary no energy absorption can occur. For the very special value of Q_m given in equation 82, no reflection occurs. The incident wave m th component simply wheels in counter rotating m lobed pairs around the obstacle, oblivious of it. A relevant discussion appears in Morse and Ingard (1968) page 426.

3.7 Some Predictions

By comparing the expressions for Q_m it is possible to predict the general scattering trends of Arthur's Island. For example, $-\sqrt{1 - \frac{m^2}{K_o^2}}$ equals -1 for the zero order mode. Thus Arthur's Island is a black body for this mode. For the next few modes $-\sqrt{1 - \frac{m^2}{K_o^2}}$ is near -1 so Arthur's Island must tend to resemble a black body. But the first few modes carry most of the energy in a plane wave. Thus Arthur's Island must have an absorptive cross section which tends to resemble that of a black body and these cross sections should converge for large K_o . A similar argument should apply to the scattering cross section.

For any mode for which $K_o < m$ the admittance of Arthur's Island, and hence its Q_m become purely imaginary so no energy can be absorbed by any of the relatively feeble higher order modes. It will now be shown that no appreciable energy is scattered either because Arthur's Island is very nearly perfectly transparent to all the higher order modes.

To prove this assertion it is only necessary to show that

$$\sqrt{\frac{m^2}{K_o^2} - 1} \text{ approaches } \frac{J'_m(K_o)}{J_m(K_o)}$$

for m greater than K_o , as follows

$$\sqrt{\frac{m^2}{K_o^2} - 1} = \frac{m}{K_o} \sqrt{1 - \frac{K_o^2}{m^2}}$$

$$= \frac{m}{K_o} \left(1 - \frac{1}{2} \frac{K_o^2}{m} - \frac{1}{2} \frac{1}{4} \frac{K_o^4}{m} + + \right) \tag{83}$$

Now retain only the first two terms of the power series.

$$\sqrt{\frac{m^2}{K_o^2} - 1} \rightarrow \frac{m}{K_o} - \frac{1}{2} \frac{K_o}{m}$$

By identity

$$K_o J'_m(K_o) = m J_m(K_o) - J_{m+1}(K_o) \tag{84}$$

$$\frac{J'_m(K_o)}{J_m(K_o)} = \frac{m}{K_o} - \frac{J_{m+1}(K_o)}{J_m(K_o)} \tag{85}$$

A power series expansion for $J_m(K_o)$ is,

$$J_m(K_o) = \frac{(\frac{1}{2} K_o)^m}{m!} - \frac{(\frac{1}{2} K_o)^{m+2}}{(m+1)!} + + \tag{86}$$

Similarly expand $J_{m+1}(K_o)$, retain only the first terms and form their ratio.

$$\frac{J'_m(K_o)}{J_m(K_o)} \rightarrow \frac{m}{K_o} - \frac{1}{2} \frac{K_o}{m}$$

Thus

$$Q_m \text{ Arthur's Island} \rightarrow Q_m \text{ Transparent Body} \tag{87}$$

As m exceeds K_o

The question of how rapidly these two expressions converge was examined numerically. The convergence is indeed very rapid as shown in Figure 11. Beyond a first transition mode for which m is first greater than K_o , Arthur's Island is essentially transparent. It is thus predictable that the scattering, absorption, and total cross sections of Arthur's Island are all somewhat smaller than those of a black body but approach those of a black body as K_o increases.

11

THE TRANSPARENCY OF ARTHUR'S ISLAND TO NON-PROPAGATING MODES

Arthur's Island exhibits an unexpected transparency to all higher order (non-propagating) modes. Thus they are not reflected.

TABLE 1

CROSS SECTIONS

For spheres:

Morse NotationGeorge Notation

$$\begin{aligned} \sum_S &= \frac{\pi}{k^2} \sum_m (2m+1) |1 + R_m|^2 & \frac{4\pi}{k^2} \sum_m (2m+1) |A_m|^2 \\ \sum_a &= \frac{\pi}{k^2} \sum_m (2m+1) (1 - |R_m|^2) & \frac{4\pi}{k^2} \sum_m (2m+1) (-1) [|A_m|^2 + \text{Re } A_m] \\ \sum &= \frac{2\pi}{k^2} \sum_m (2m+1) (1 + \text{Re } R_m) & \frac{4\pi}{k^2} \sum_m (2m+1) [-\text{Re } A_m] \end{aligned}$$

Similarly, for the cylinder

Morse NotationGeorge Notation

$$\begin{aligned} \sum_S &= \frac{1}{2k} \sum_m (2 - \delta_{m0})^2 |1 + R_m|^2 & \frac{2}{k} \sum_m (2 - \delta_{m0})^2 |A_m|^2 \\ \sum_a &= \frac{1}{2k} \sum_m (2 - \delta_{m0})^2 (1 - |R_m|^2) & \frac{2}{k} \sum_m (2 - \delta_{m0})^2 (-1) [|A_m|^2 + \text{Re } A_m] \\ \sum &= \frac{1}{k} \sum_m (2 - \delta_{m0})^2 (1 + \text{Re } R_m) & \frac{2}{k} \sum_m (2 - \delta_{m0})^2 (-\text{Re } A_m) \end{aligned}$$

The summations extend from $m = 0$ to $m = +\infty$.

See definitions in Section 3.6

4.0 NUMERICAL RESULTS

4.1 Cross Sections

The scattering, absorption, and total cross sections as presented in Section 3, were calculated for K_0 ranging from 0.1 to 11.0 in increments of 0.1. This was done for Arthur's Island and the three reference cases, a hard body of zero admittance, a soft body of infinite admittance, and a black body of unit admittance. The results are presented in Figures 12, 13 and 14.

Figure 12 shows the scattering cross section for all four cases. Arthur's Island scatters the least. Its cross section comprises a series of peaks which approach the black body scattering as each new mode "cuts on," then subsides somewhat until another mode "cuts-on." The scattering cross sections of Arthur's Island and the black body converge slowly as K_0 increases.

As is well known, the soft body scattering cross section greatly exceeds that of the rigid body for small values of K_0 but the two converge slowly as K_0 increases.

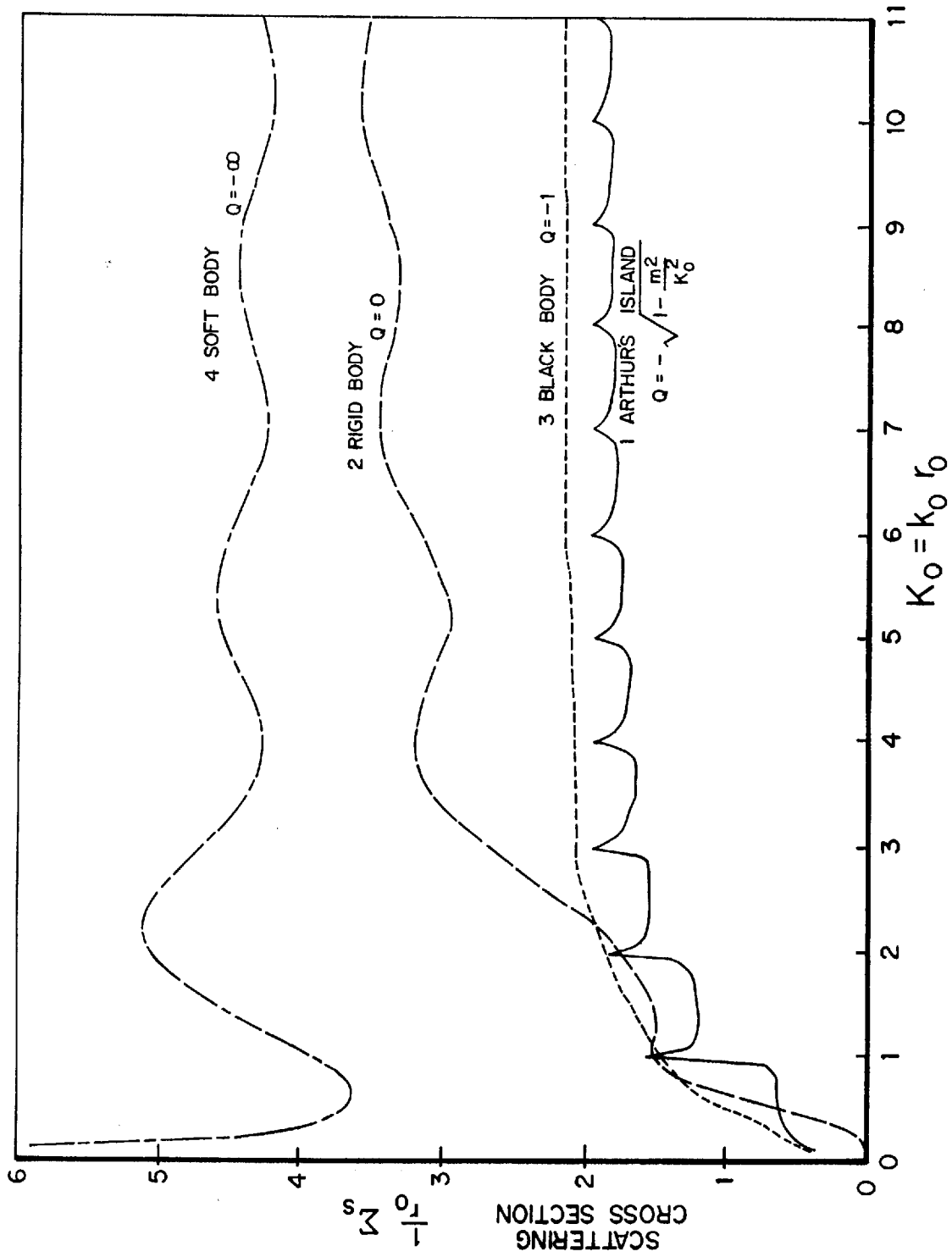
Figure 13 presents the absorption cross section for Arthur's Island and the black body. The black body exhibits a broad peak near $K_0 = 1$, then the absorption cross section gradually settles towards an asymptotic value of 2 (radii) as K_0 becomes large.

The absorption cross section of Arthur's Island comprises a series of peaks and valleys of diminishing amplitude and approaching the black body curve as K_0 increases. Whereas the scattering peaks of Arthur's Island occur at integral values of K_0 , the absorption peaks occur for values of K_0 a little larger than an integer. For example, scattering peaks at $K_0 = 3$ but absorption peaks at about $K_0 = \pi$.

12

SCATTERING CROSS SECTIONS VS. K_0 FOR SOFT, HARD,
AND BLACK CYLINDERS AND ARTHUR'S ISLAND

Arthur's Island scatters the least due partly to its transparency to higher order modes. The scattering peaks occur at integral values of K_0 .

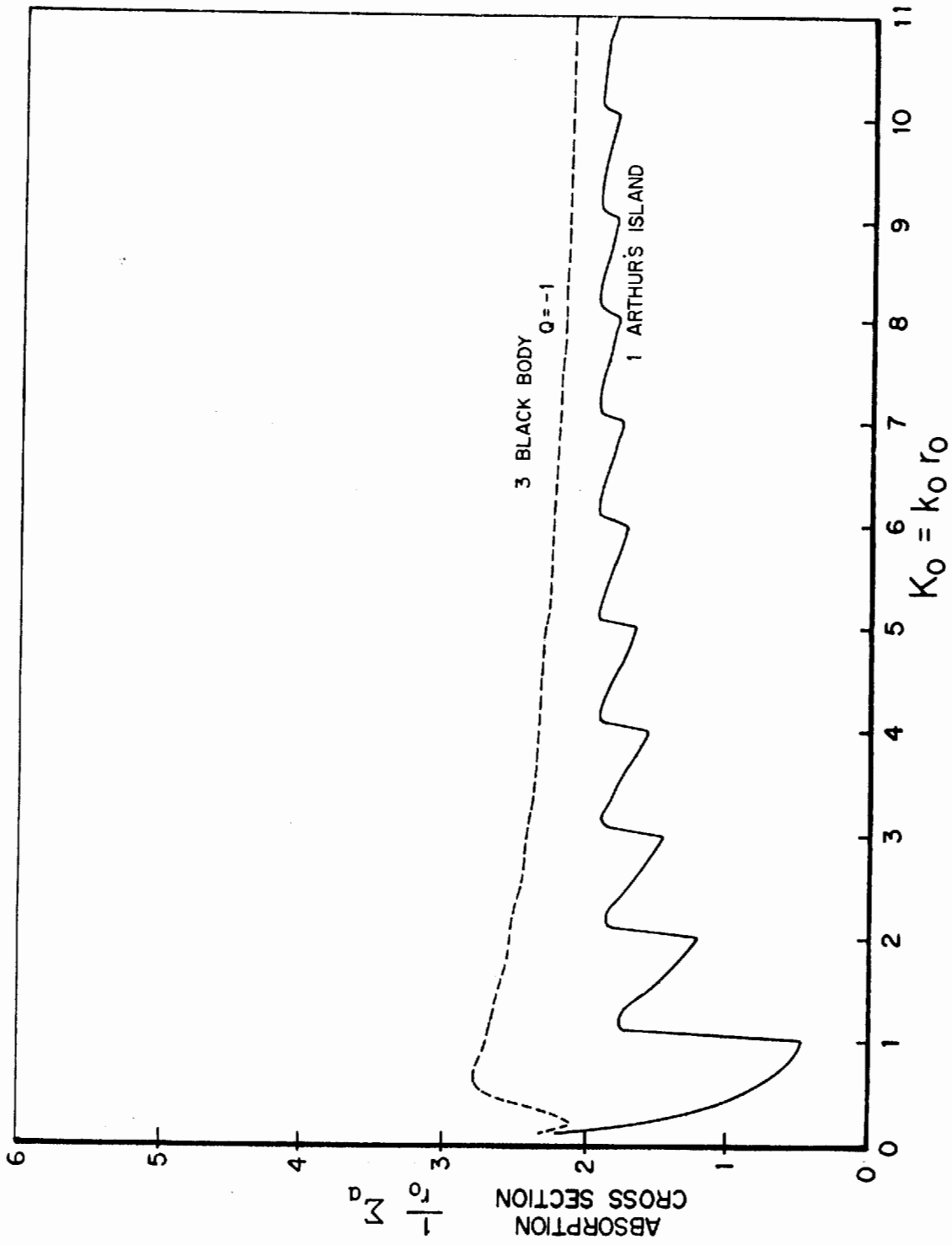


13

ABSORPTION CROSS SECTIONS VS. K_0 FOR THE BLACK BODY
AND ARTHUR'S ISLAND

The absorptive peaks occur for K_0 a little larger
than an integer as each new mode becomes well

"cut-on."



14

—————
TOTAL CROSS SECTIONS VS. K_0

These curves were computed as shown in Table 1 but they may also be obtained by adding Figures 12 and 13.

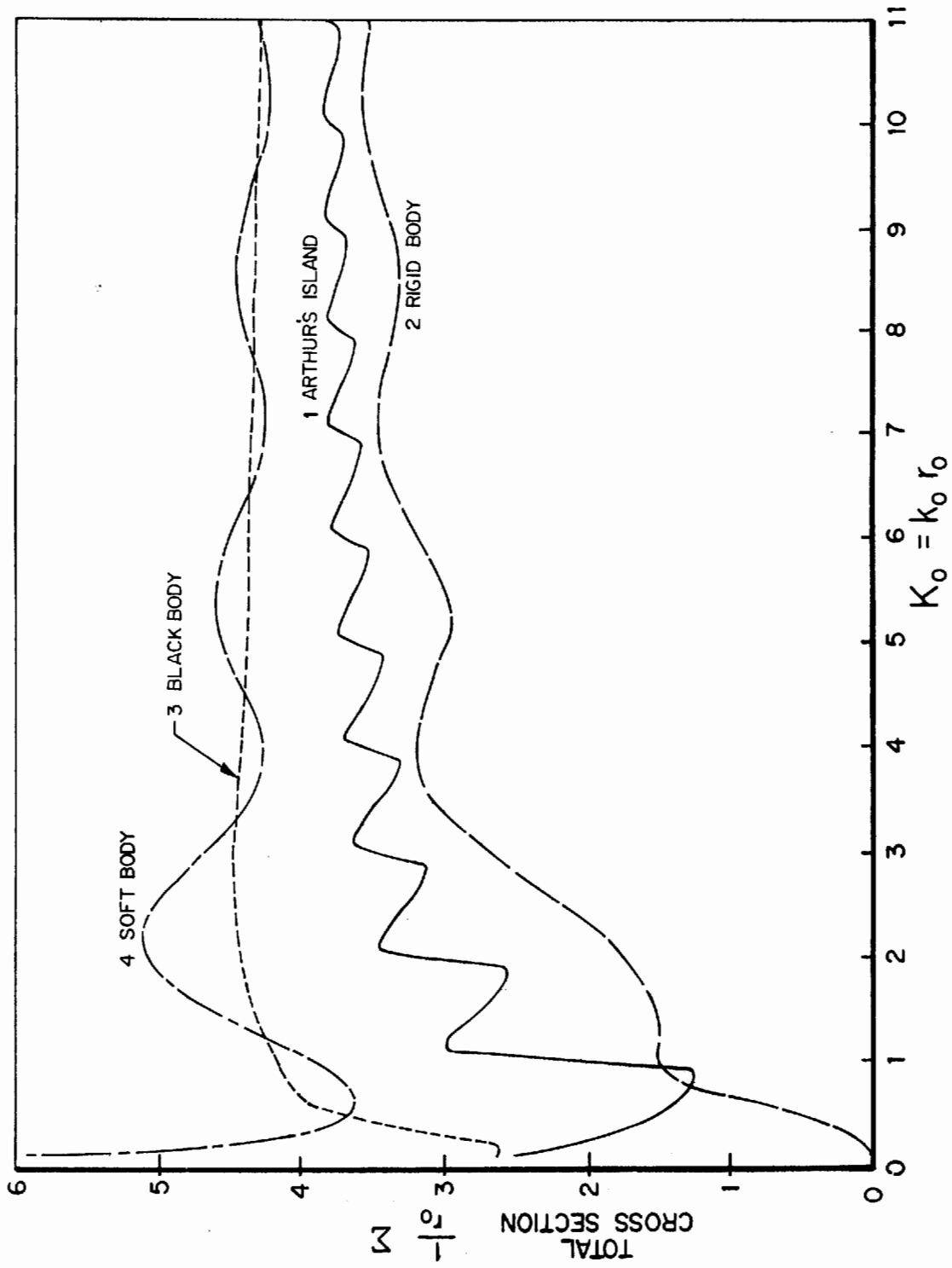


Figure 14 displays the total cross section for all four cases. The total cross section of the rigid body is the least. The total cross section of Arthur's Island moderately exceeds that of the rigid body everywhere except for a dip near $K_0 = 1$. The total cross section of the black body and the soft body are generally similar but the soft body curve undulates in a damped manner about the more regular black body curve. All four appear headed for convergence for very large K_0 .

One potential usefulness of the absorption cross sections is to facilitate tradeoff studies in the design of wave energy extraction devices of the wave focusing type. The surface area, and hence the amount of material required, increases as the square of the radius, whereas the energy absorption increases more nearly in proportion to the radius. Thus the efficiency per unit of construction material becomes progressively greater as K_0 decreases, in spite of the decreasing absorption cross section, so tradeoff studies become necessary.

4.2 Differential Scattering

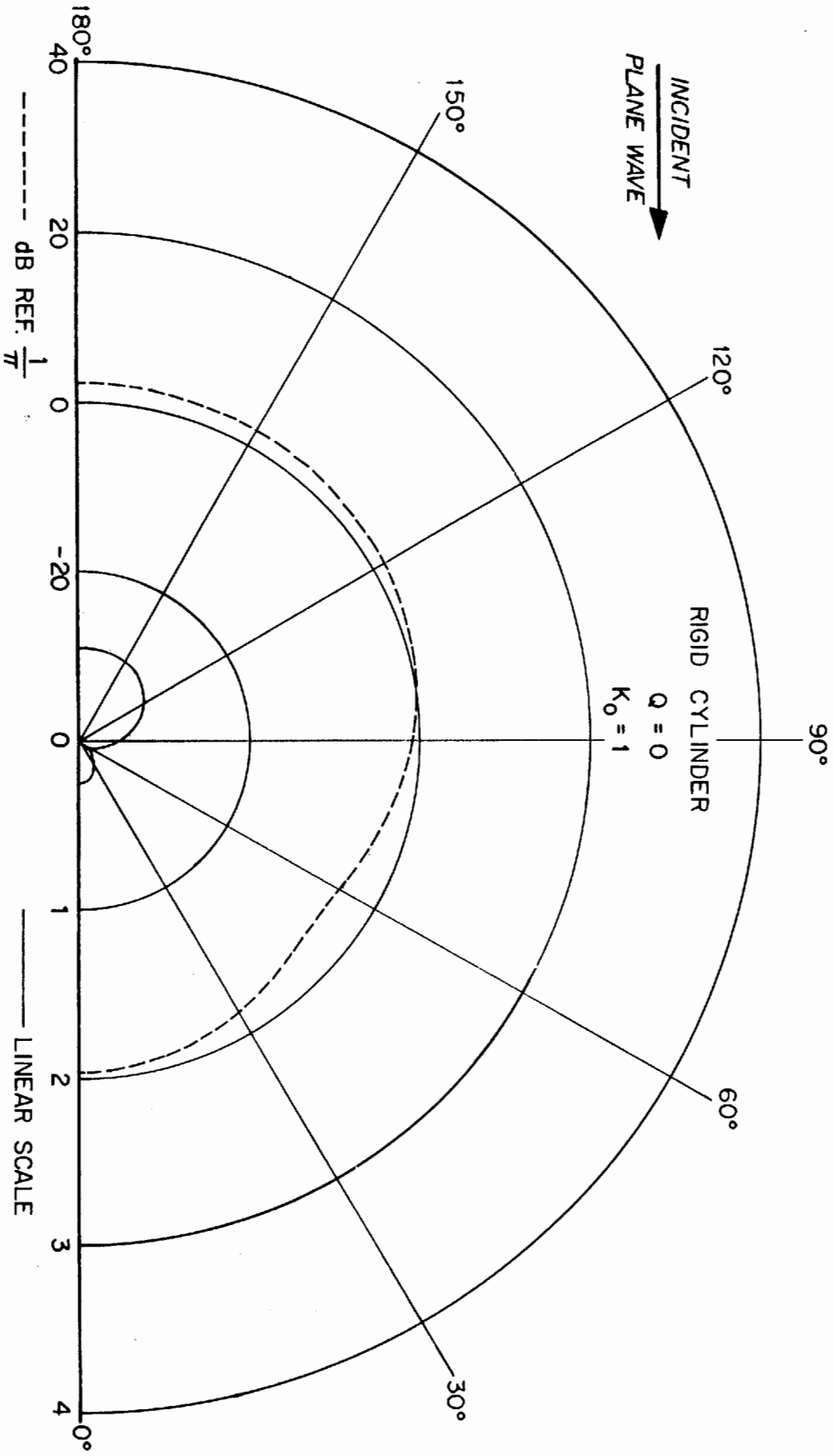
Equation 61 provides the polar distribution of the differential scattering. The amplitude variations are so great that a decibel scale is useful. The reference level chosen is $\frac{1}{\pi}$. Thus zero dB is the differential scattering which, if uniform around 360° would correspond to a cross section of two radii. The figures also show the same data on a linear scale. Viewed on a linear scale the lobes are much more dramatic.

Figure 15 presents a polar plot of differential scattering for rigid body $K_0 = 1$. The generally backward scattering reflection in the second quadrant, is somewhat enhanced. The lobe of interfering radiation in the positive direction, first quadrant, is not yet fully developed. Figure 16 represents a much larger rigid body, $K_0 = 20$. The second quadrant reflected energy is still a little enhanced. The first quadrant now shows a developed interference lobe plus a fine structure of sharp lesser lobes. These are familiar patterns to students of scattering and serve mainly to validate the methodology.

15

DIFFERENTIAL SCATTERING FOR A SMALL HARD CYLINDER

$$K_0 = 1, Q = 0$$



16

DIFFERENTIAL SCATTERING FOR A LARGE HARD CYLINDER

$$K_o = 20, Q = 0$$

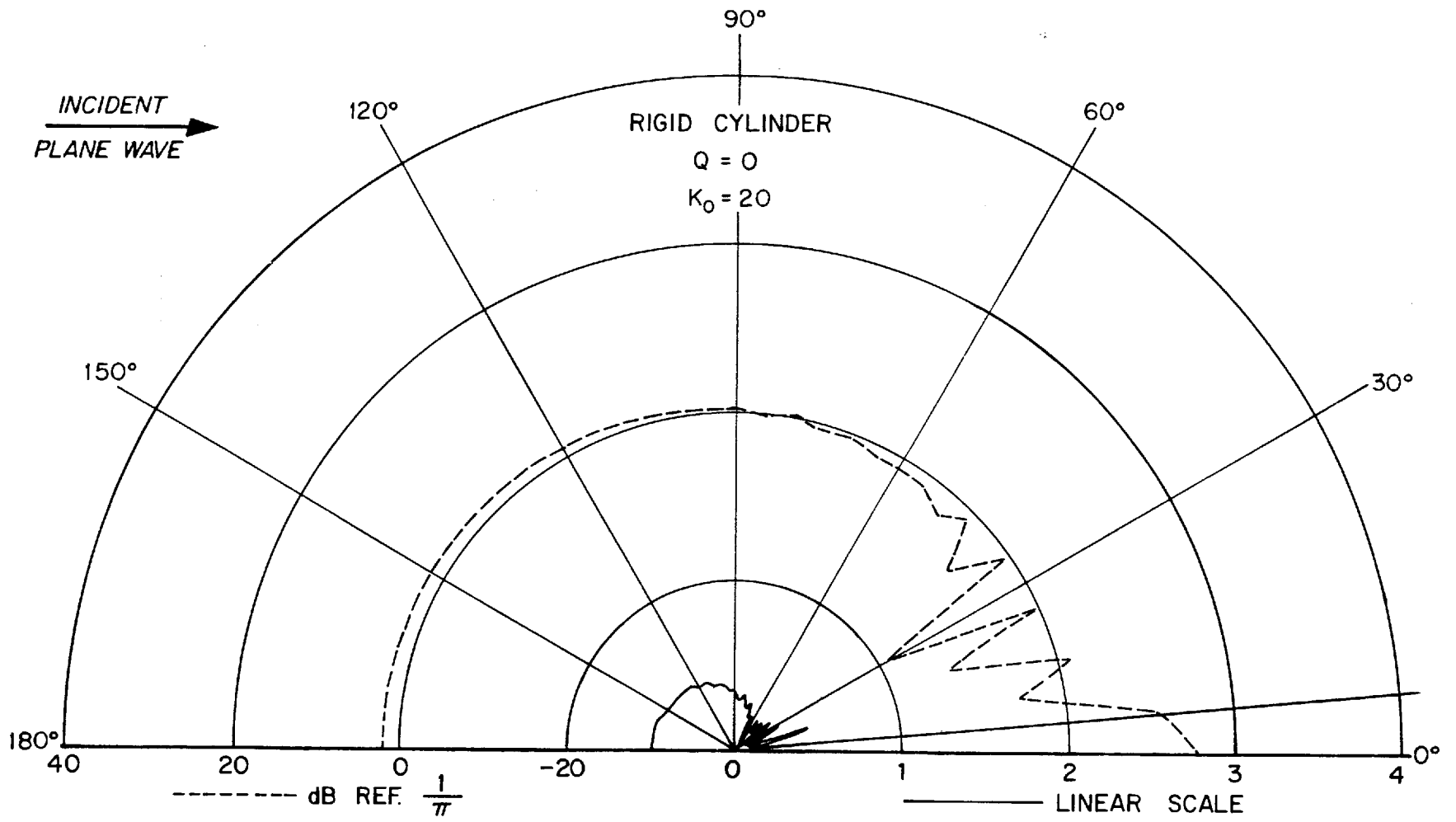


Figure 17 shows the differential scattering from a small soft body, $K_0 = 1$. The second quadrant reflection is much like that of the rigid body but the interference lobe is much larger. This accounts for the much larger scattering cross section shown in Figure 12. The scattering pattern for the large soft body, $K_0 = 20$, shown in Figure 18 is very similar to that for the rigid body except that the minor lobes in the first quadrant are much subdued.

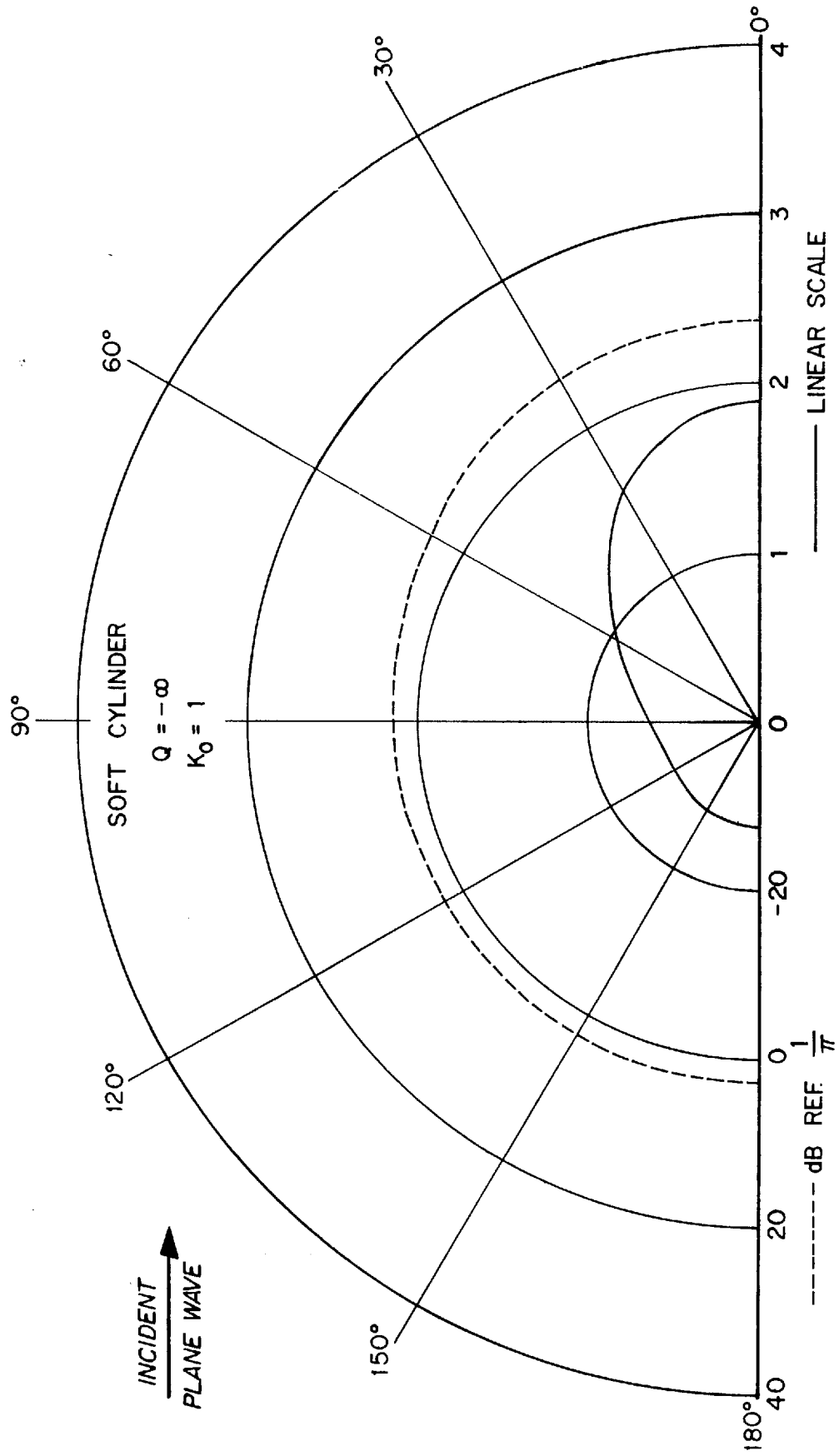
The polar plots of differential scattering for the black body differ greatly from those of the rigid or soft body. Figures 19, 20, and 21 apply to the black body for $K_0 = 1, 3.6,$ and 20 respectively. All are generally cardioid in shape with a very pronounced minimum at $\theta = \pi$ (sonar backscattering) and a maximum forming the interference lobe at $\theta = 0$. The minor lobes are not at all sharp. These patterns will be closely compared to those of Arthur's Island.

The polar plots of differential scattering for Arthur's Island clearly show the cut-on of individual modes. Figure 22 presents the differential scattering for the case $K_0 = .9$ for which only the zero order mode can propagate across the island. The scattered energy is uniform in all directions. For $K_0 = 1$ the onset of the first order mode occurs and the scattering pattern changes abruptly to a nearly symmetrical double ended pattern with slightly enhanced reflection and the beginnings of an interference lobe as shown in Figure 23. For the case $K_0 = 3.6$ shown in Figure 24 there is a considerable resemblance to a black body of the same size in Figure 20. Each exhibits four lobes and the interference lobes (shadow) are very similar. Both show substantial attenuation in the second quadrant reflection. The back scatter at $\theta = \pi$, is greater for Arthur's Island than for the black body. Figure 25 presents the scattering pattern for Arthur's Island with $K_0 = 20$. This shows considerable resemblance to the same size of black body in Figure 21. The main interference lobes at $\theta = 0$ are very similar and this similarity continues for most of the first quadrant. In the second quadrant Arthur's Island shows a very complex system of minor lobes as contrasted to their complete absence for the black body. The back scatter at $\theta = \pi$ is weak (-12 dB) but much greater than for the black body (-40 dB).

17

DIFFERENTIAL SCATTERING FOR A SMALL SOFT CYLINDER

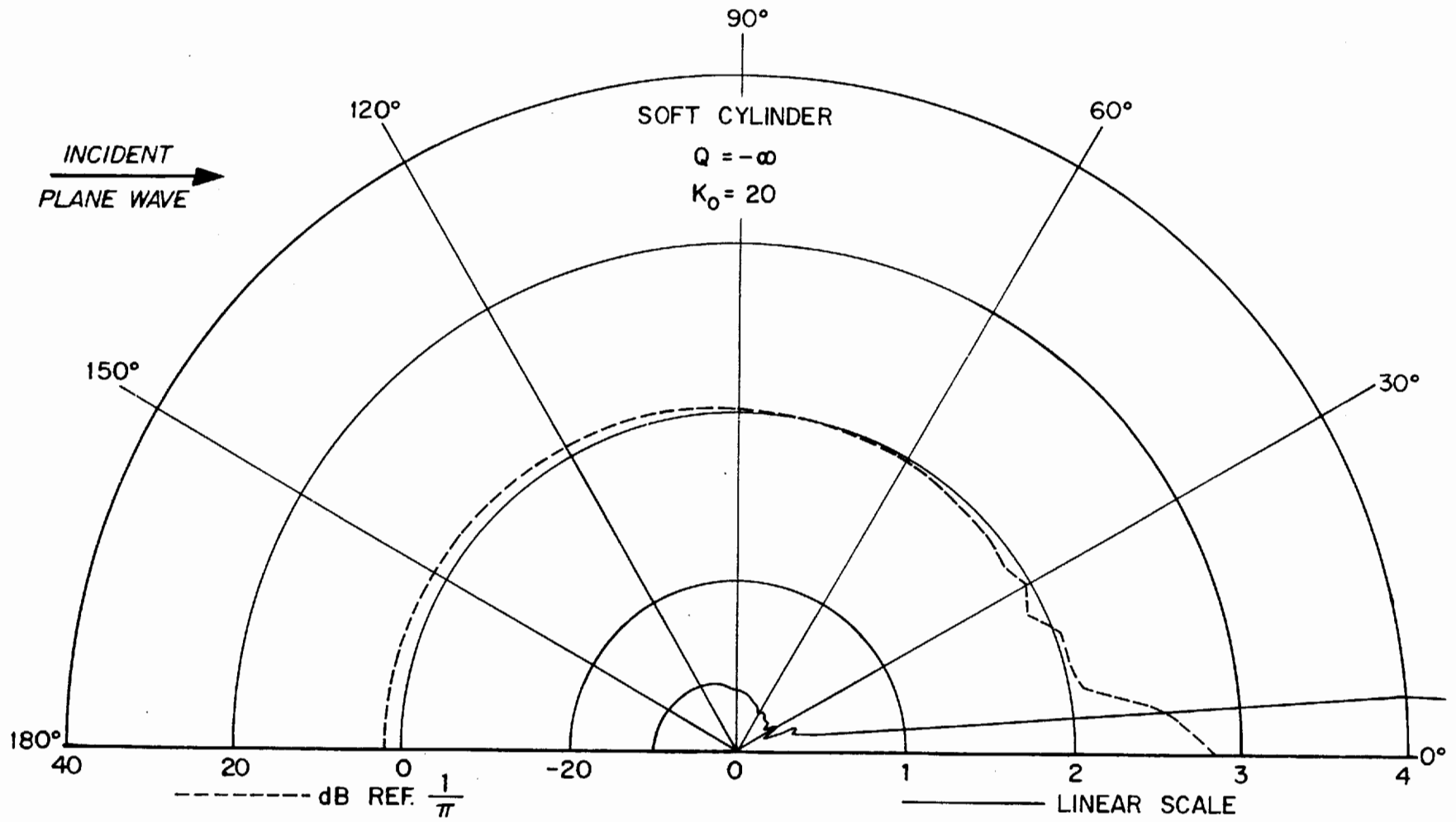
$$K_0 = 1, Q = -\infty$$



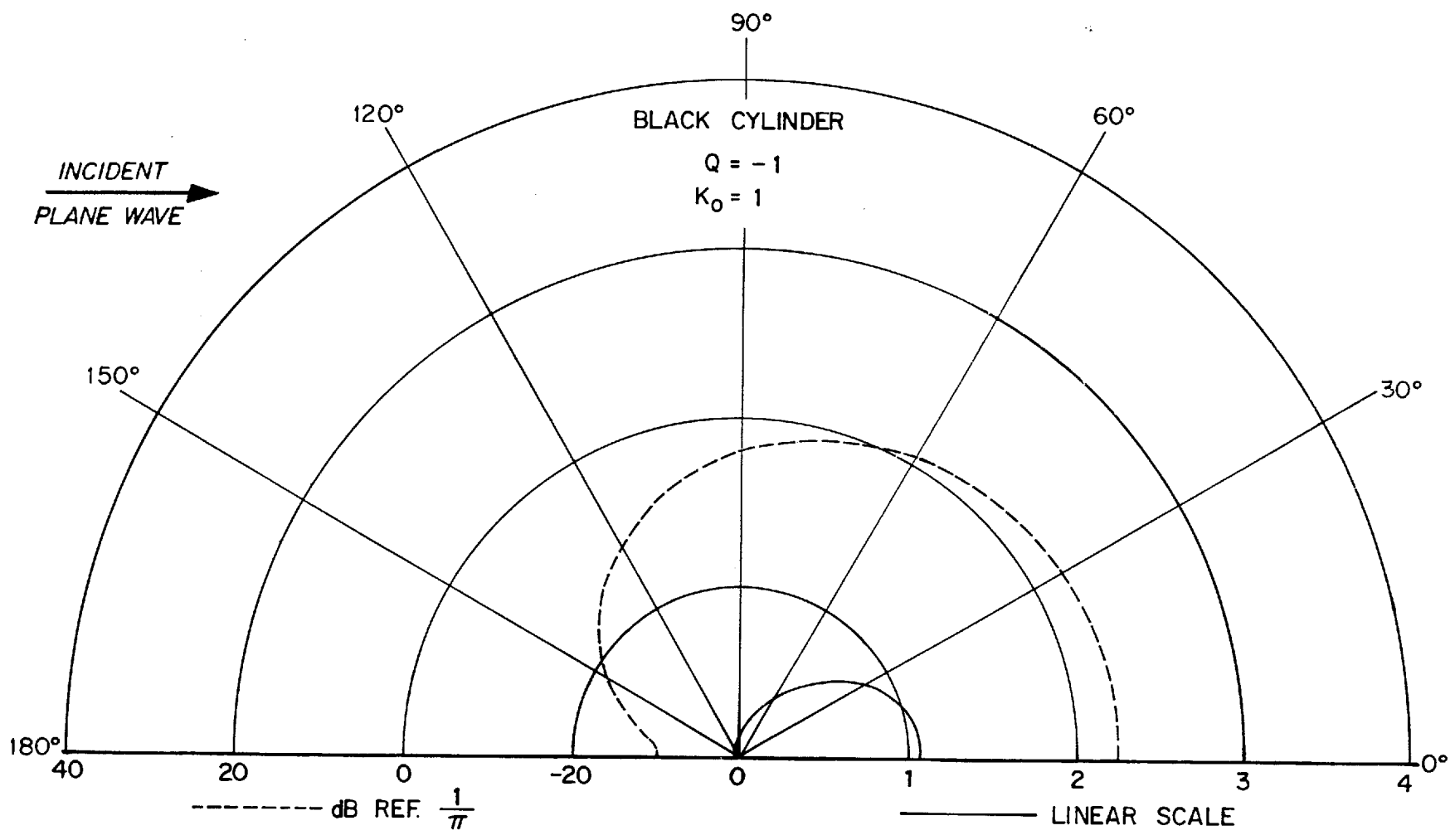
18

DIFFERENTIAL SCATTERING FOR A LARGE SOFT CYLINDER

$$K_0 = 20, Q = -\infty$$



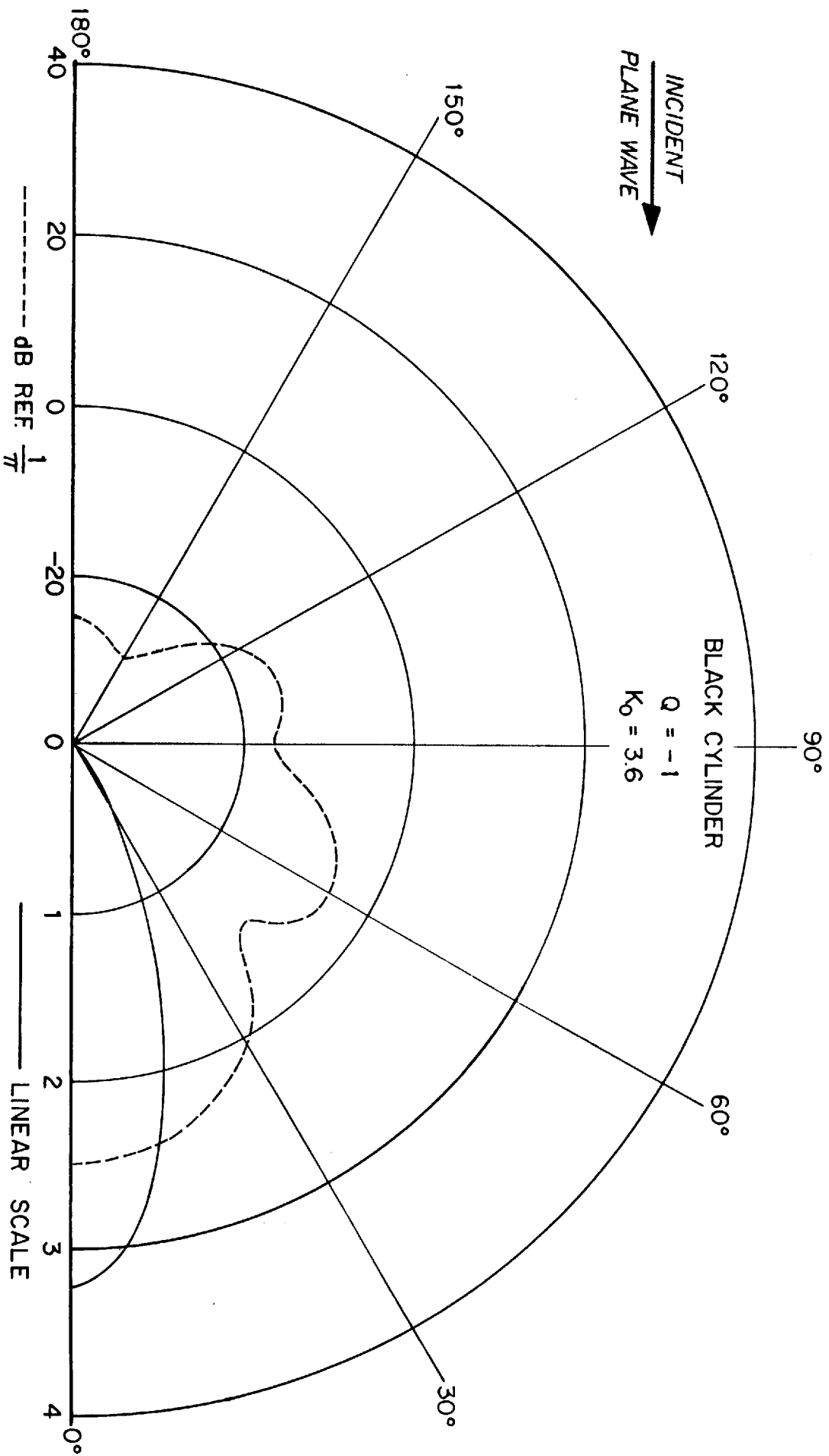
DIFFERENTIAL SCATTERING FOR A SMALL BLACK CYLINDER
 $K^0 = 1, Q = -1$



20

DIFFERENTIAL SCATTERING FOR A MEDIUM SIZED BLACK
CYLINDER

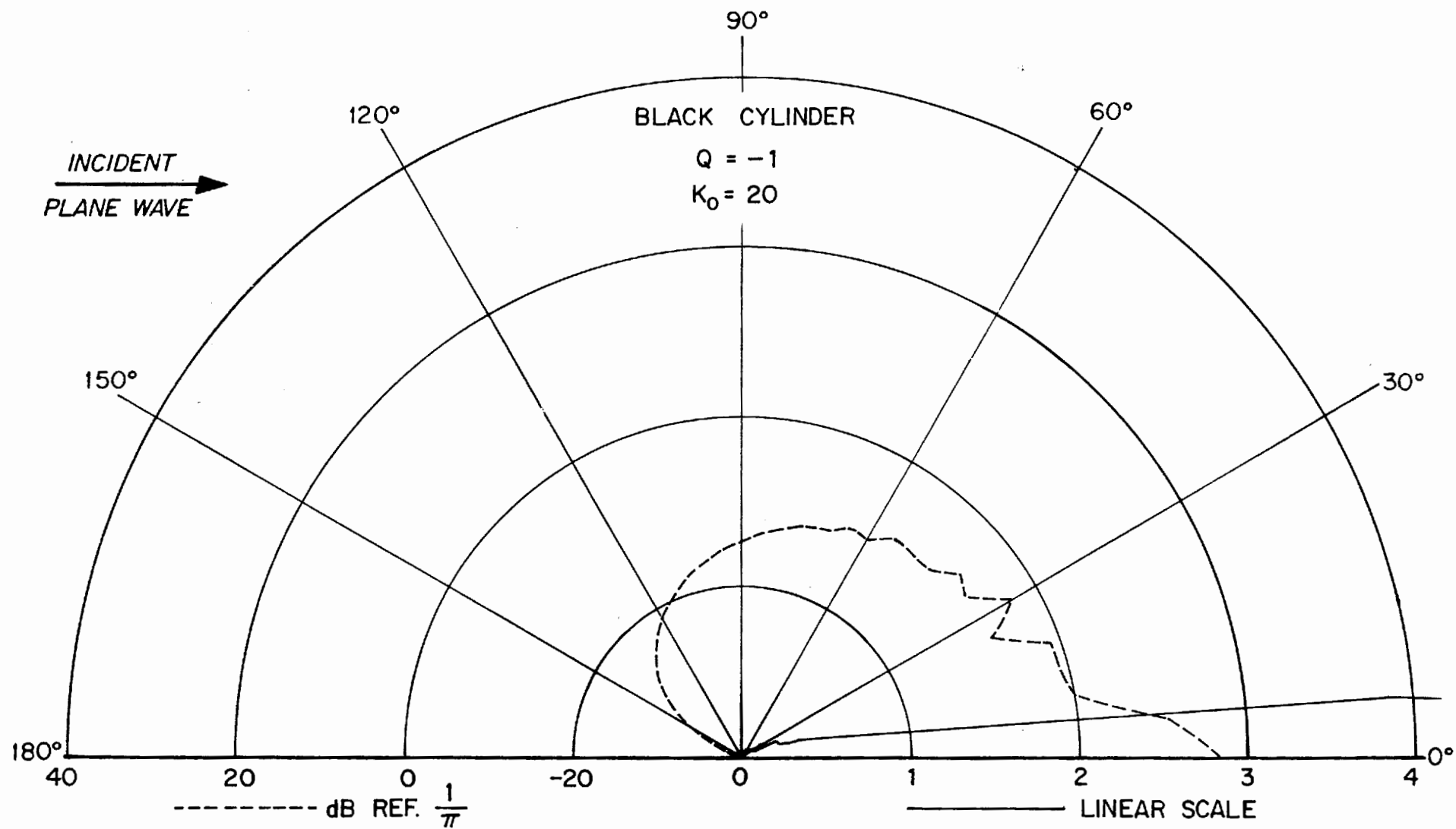
$$K_o = 3.6, Q = -1$$



21

DIFFERENTIAL SCATTERING FOR A LARGE BLACK CYLINDER

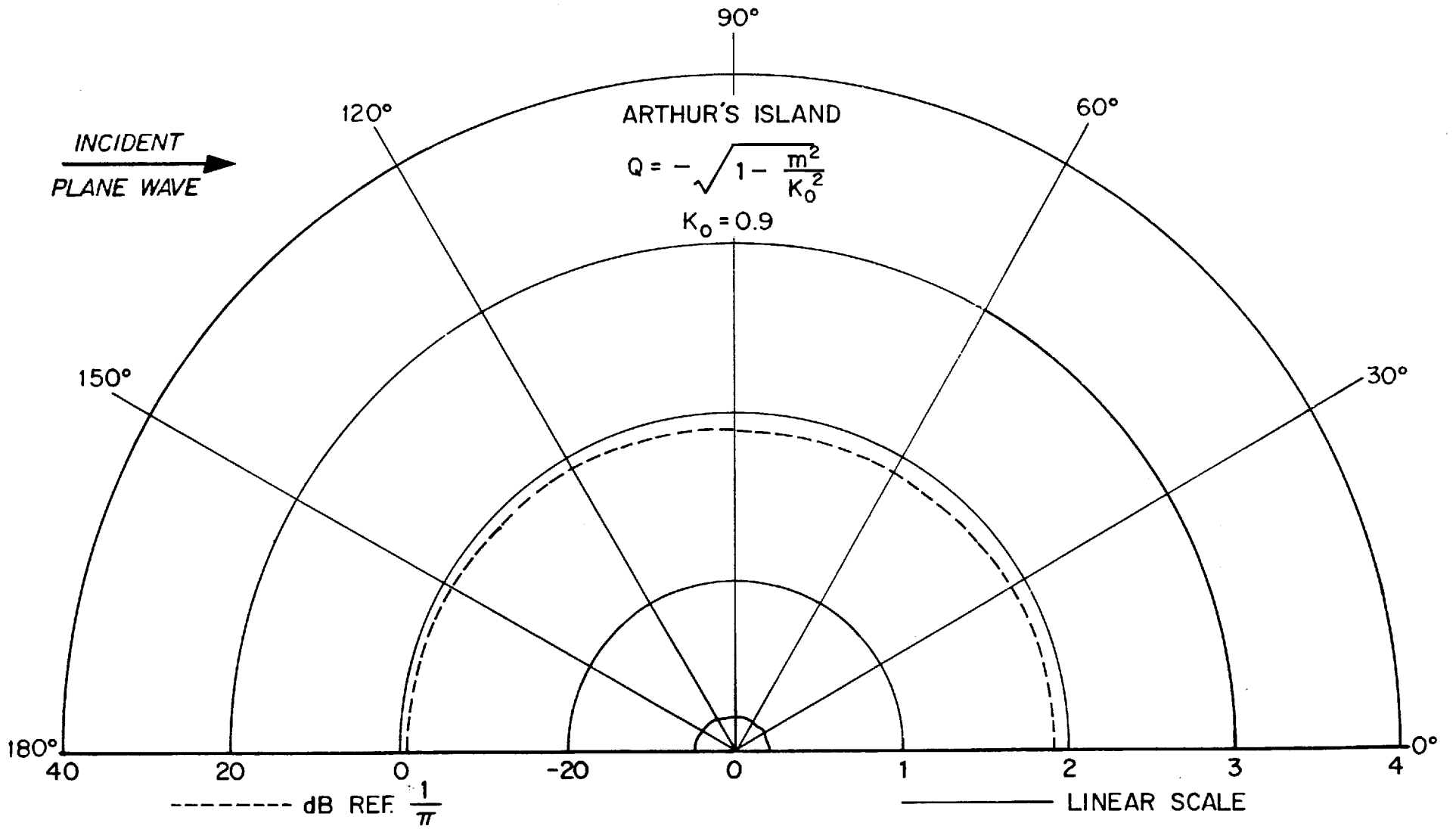
$$K_0 = 20, Q = -1$$



22

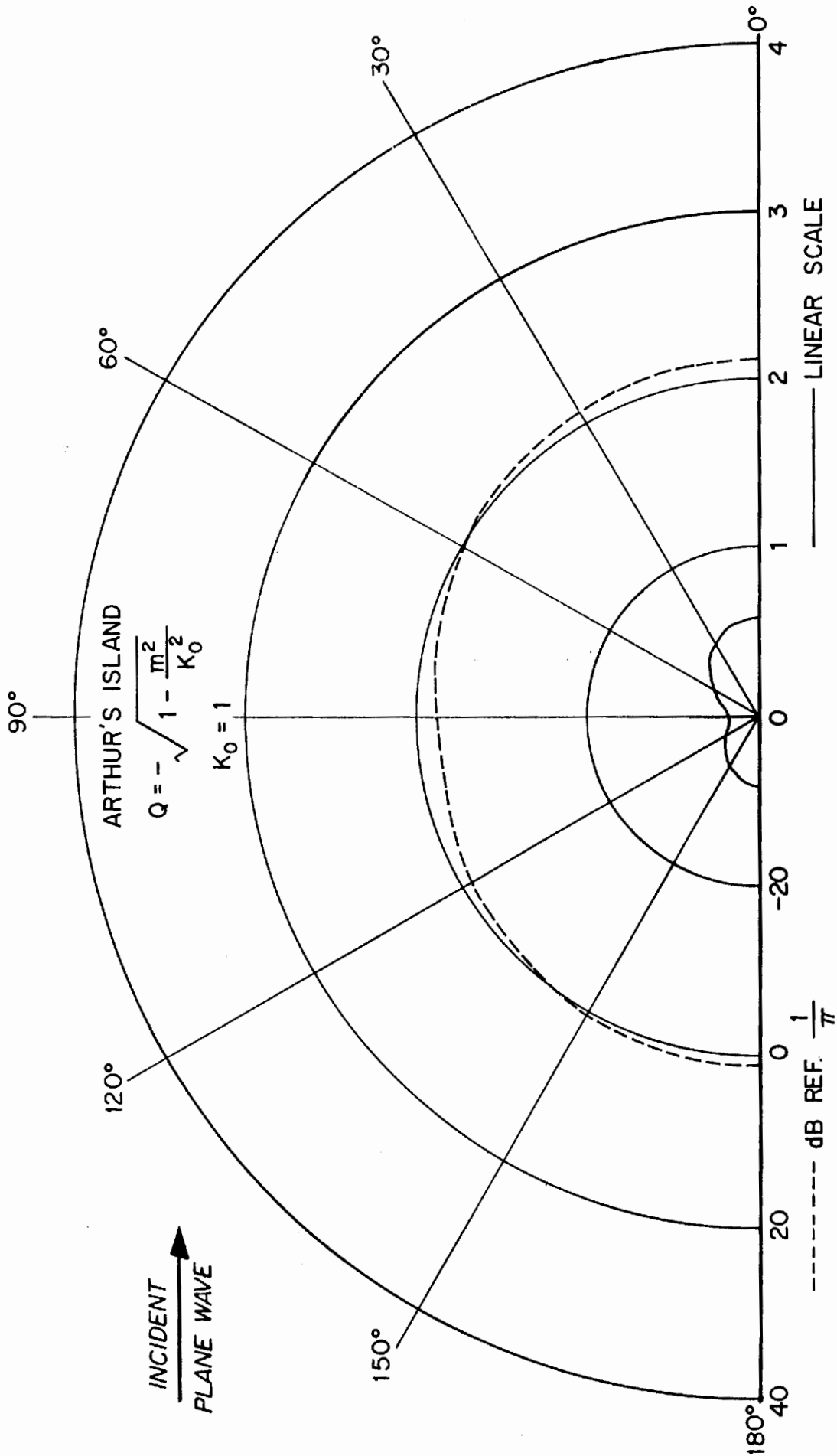
DIFFERENTIAL SCATTERING FOR A VERY SMALL ARTHUR'S
ISLAND

$$K_o = 0.9, Q_m = -\sqrt{K_o^2 - m^2}$$



DIFFERENTIAL SCATTERING FOR A SMALL ARHTUR'S ISLAND

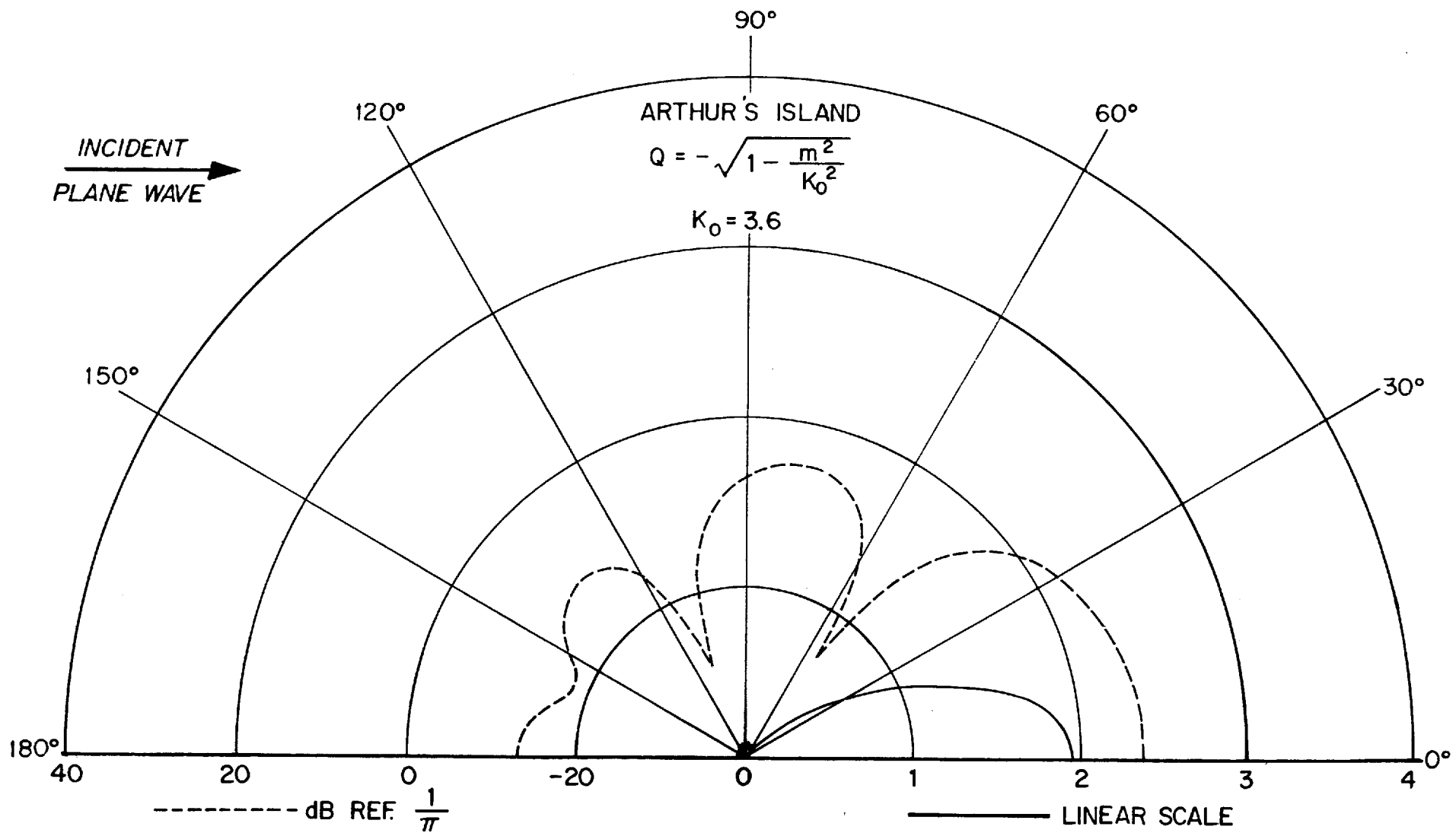
$$K_o = 1, O_m = \sqrt{\frac{K_o^2 - m^2}{2}}$$



24

DIFFERENTIAL SCATTERING FOR A MEDIUM SIZED
ARTHUR'S ISLAND

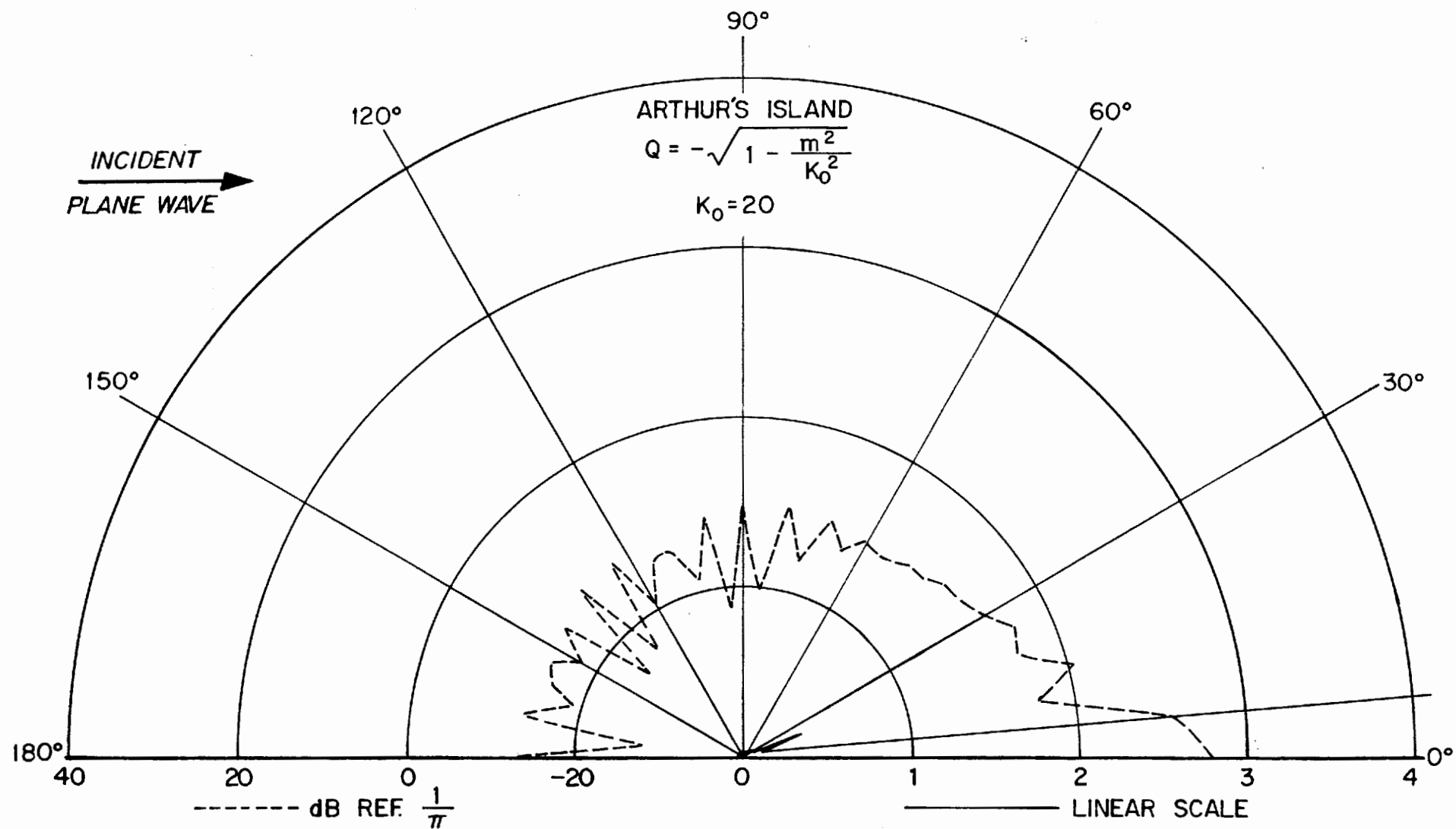
$$K_o = 3.6, Q_m = -\sqrt{K_o'^2 - m^2}$$



25

DIFFERENTIAL SCATTERING FOR A LARGE ARTHUR'S
ISLAND

$$K_o = 20, Q_m = -\sqrt{K_o^2 - m^2}$$



5.0 ARTHUR'S ISLANDS WITH CLIPPED SKIRTS

5.1 Case 1; Constant r_o , Variable r_c

In all of the foregoing text the outer radius r_o has been taken to be that at which $c = c_o$, which means the depth h_o is infinite. The depth of the lip h is $.5 \lambda_o$ at $R_c = 0.996$ and this is commonly taken to be close enough to $R_o = 1.0$. Material costs are often estimated to build a dome $.5 \lambda_o$ deep. If however the dome design could be clipped off at depth $h = .25 \lambda_o$ where $R_c = 0.933$, then only about half as much material would be required.

For an island clipped at r_c the calculation of the absorption cross section normalized by r_o as a function of $k_o r_o = K_o$ is identical to that previously used for the full Arthur's Island. It is only necessary to apply the boundary conditions at r_c instead of r_o . This is accomplished by writing,

$$A_m = \frac{J_m'(K_o R_c) - i Q_m J_m(K_o R_c)}{H_m^1(K_o R_c) - i Q_m H_m^1(K_o R_c)} \quad (88)$$

(Note that $k_o r_c = K_o R_c$)

where:

$$Q_m = \frac{1}{R_c} (Q_m)_{R=1} \quad (89)$$

so

$$Q_m = -\frac{1}{R_c} \sqrt{1 - \frac{m^2}{K_o^2}} \quad (90)$$

Figure 26 shows a dome progressively clipped at $R_c = 0.996, 0.933, 0.80,$ etc.

26

ARTHUR'S ISLANDS WITH CLIPPED SKIRTS

Much construction material can be saved by optimum skirt clipping.

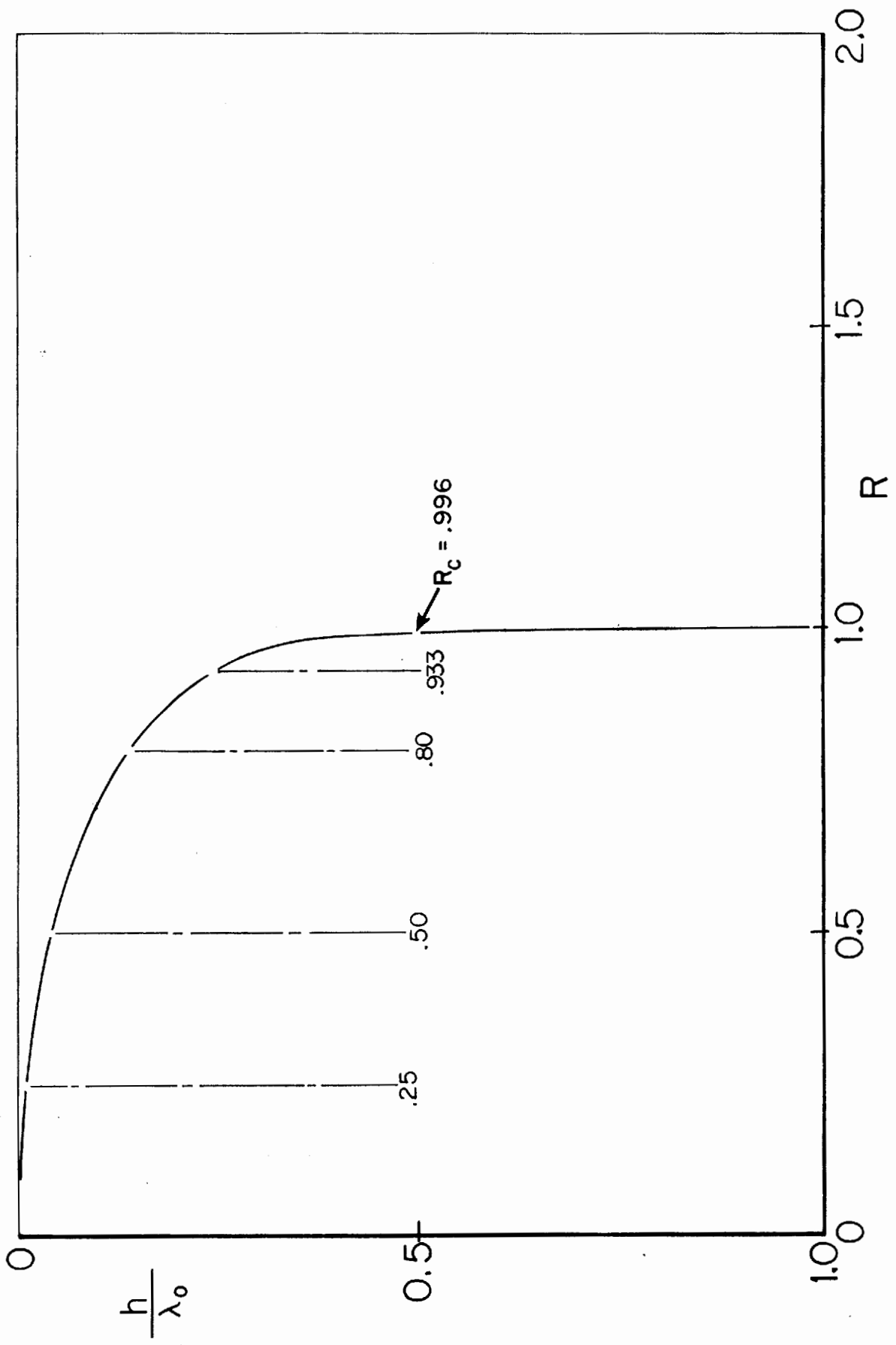


Figure 27 compares the absorption cross sections for the original island to the case $R_c = 0.9333$. The curves are very similar indeed. The response of the clipped island is shifted to the right by a factor of 1.072. This results from the change in the Bessel function argument by the factor 0.933. There is little change in shape of the peaks and valleys due to the small change in the Q_m .

Similar comments apply to Figure 28 which examines the case $R_c = 0.80$. The curves shift to the right by a factor of 1.25 but the shapes change very little.

Figure 29 shows the impact of more drastic clipping of the skirt of the island. The cases $R_c = 0.25$ and $R_c = 0.50$ are compared to the original Arthur's Island. The peaks become sparse and narrow. The valleys are deep. This shows that the change in Q_m is being felt.

5.2 Case 2; Constant r_c , Variable r_o

It is instructive to separate the effects of the change of Q_m and the change of Bessel function argument. Figure 30 shows several Arthur's Islands. These have been progressively clipped more drastically. Each has been drawn using the same value of k_o but with a different r_o such that r_c is the same for all islands. Calculation of the absorption cross sections is accomplished numerically simply by plotting the absorption cross section (normalized by r_c) vs. $k_o r_c = K_o R_c$. The results of this cross plotting are shown in Figure 31. The curves for $R_c = 0.25, 0.50, 0.80, 0.93, 1.0$ are superimposed on scales expanded by 2. Only the extreme cases $R_c = 0.25$ and 0.50 stand out due to their narrow peaks and deeper valleys. The rest very nearly lie on the curve for the original island.

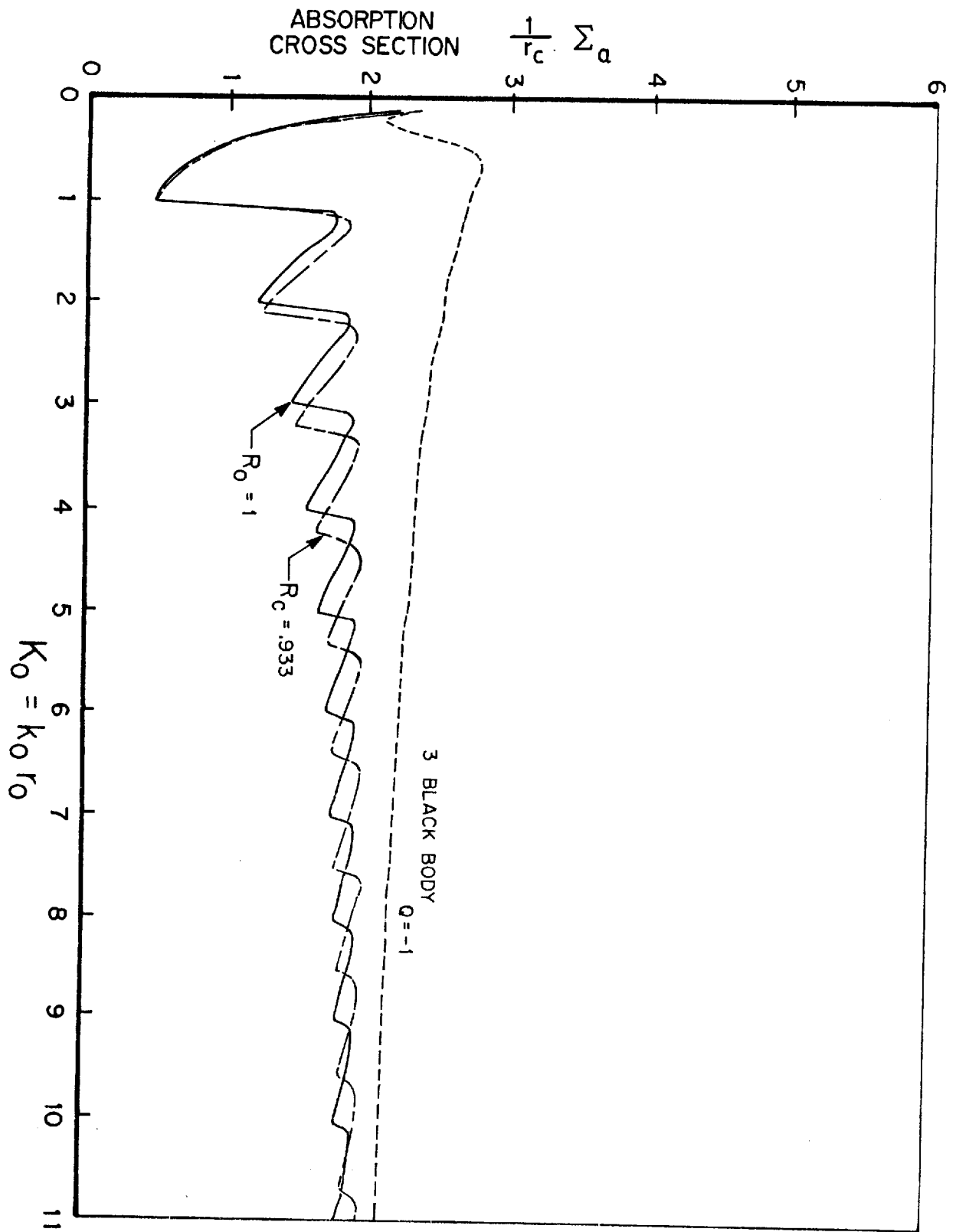
Figure 31 demonstrates that unless $R_c < 0.3$, the absorption cross section curves are substantially the same. It appears that the skirts of any Arthur's Island can be quite drastically clipped to save material, provided

that the layout values of r_o is correspondingly enlarged so that $r_c = \text{original } r_o$. This will result in major capital cost savings with negligible performance penalty.

27

ABSORPTION CROSS SECTION VS. K_0 FOR ARTHUR'S
ISLAND CLIPPED AT $R_c = .933$

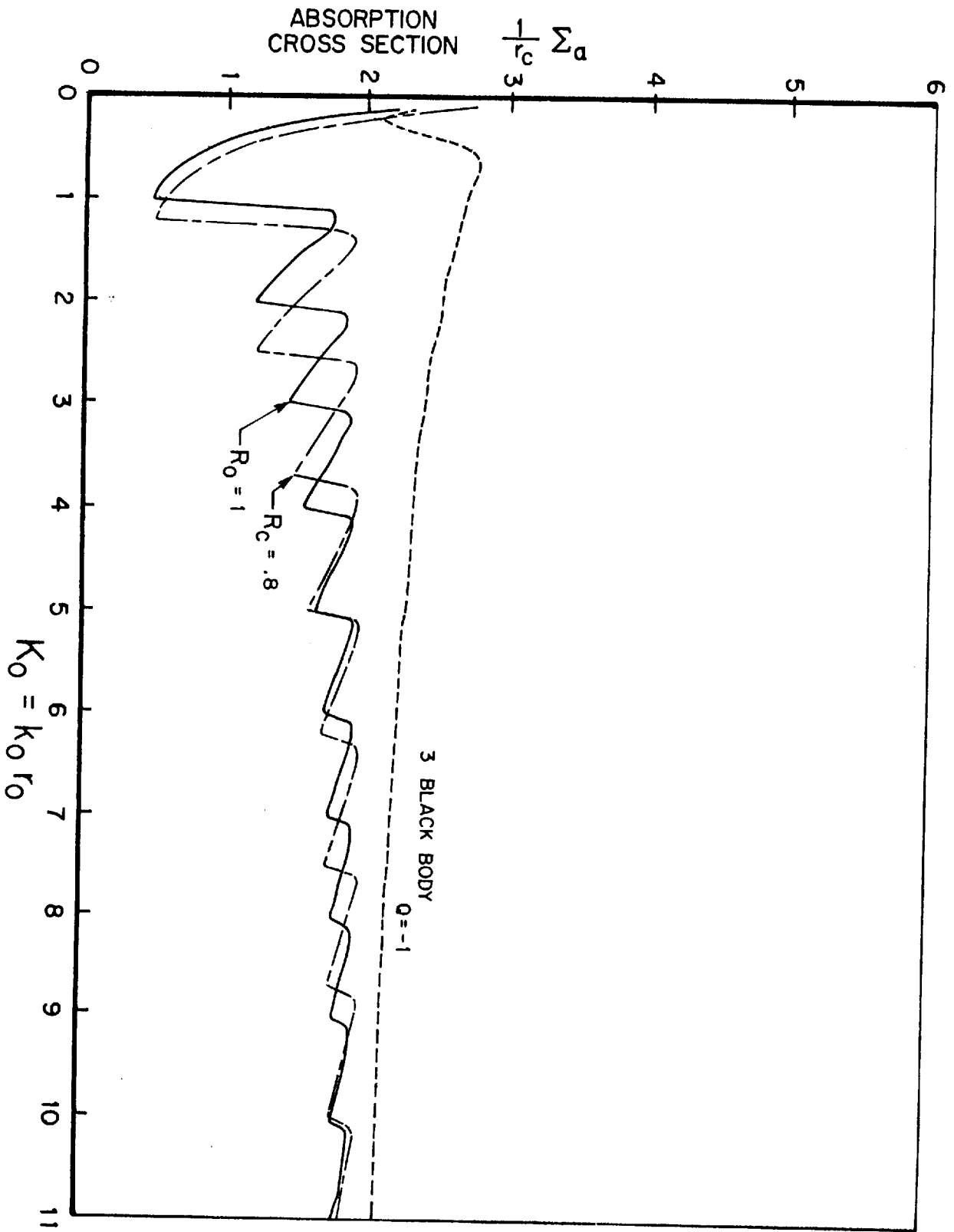
The response curve is shifted to the right by
a factor $\frac{1}{R_c}$ but very little change in shape.



28

ABSORPTION CROSS SECTION VS. K_0 FOR ARTHUR'S
ISLAND CLIPPED AT $R_c = 0.8$

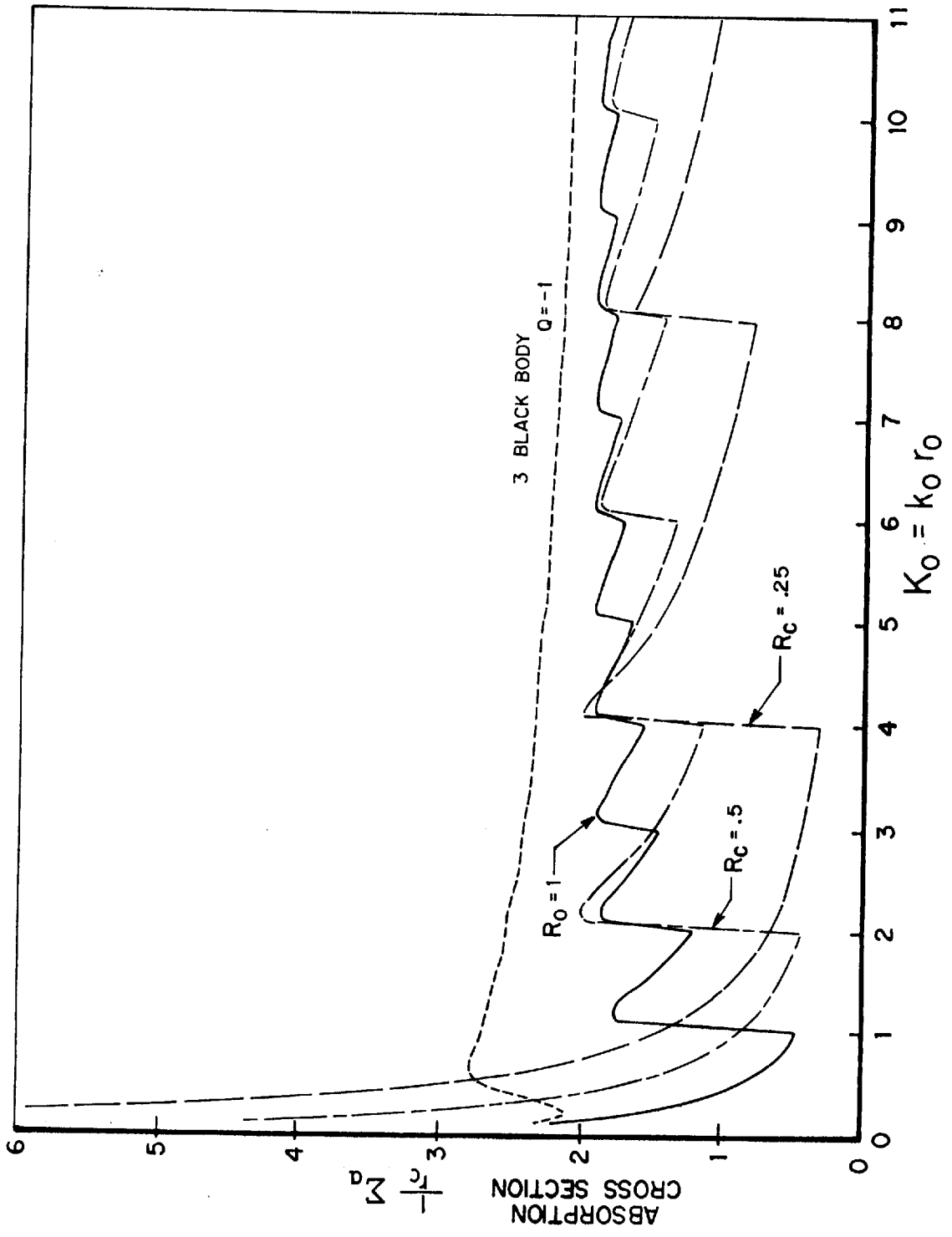
The response curve is shifted to the right
by a factor $\frac{1}{R_c} = 1.25$ but little change in
shape occurs.



29

ABSORPTION CROSS SECTION VS. K_0 FOR ARTHUR'S
ISLAND WITH DRASTIC SKIRT CLIPPING AT $R_c =$
0.5 AND 0.25

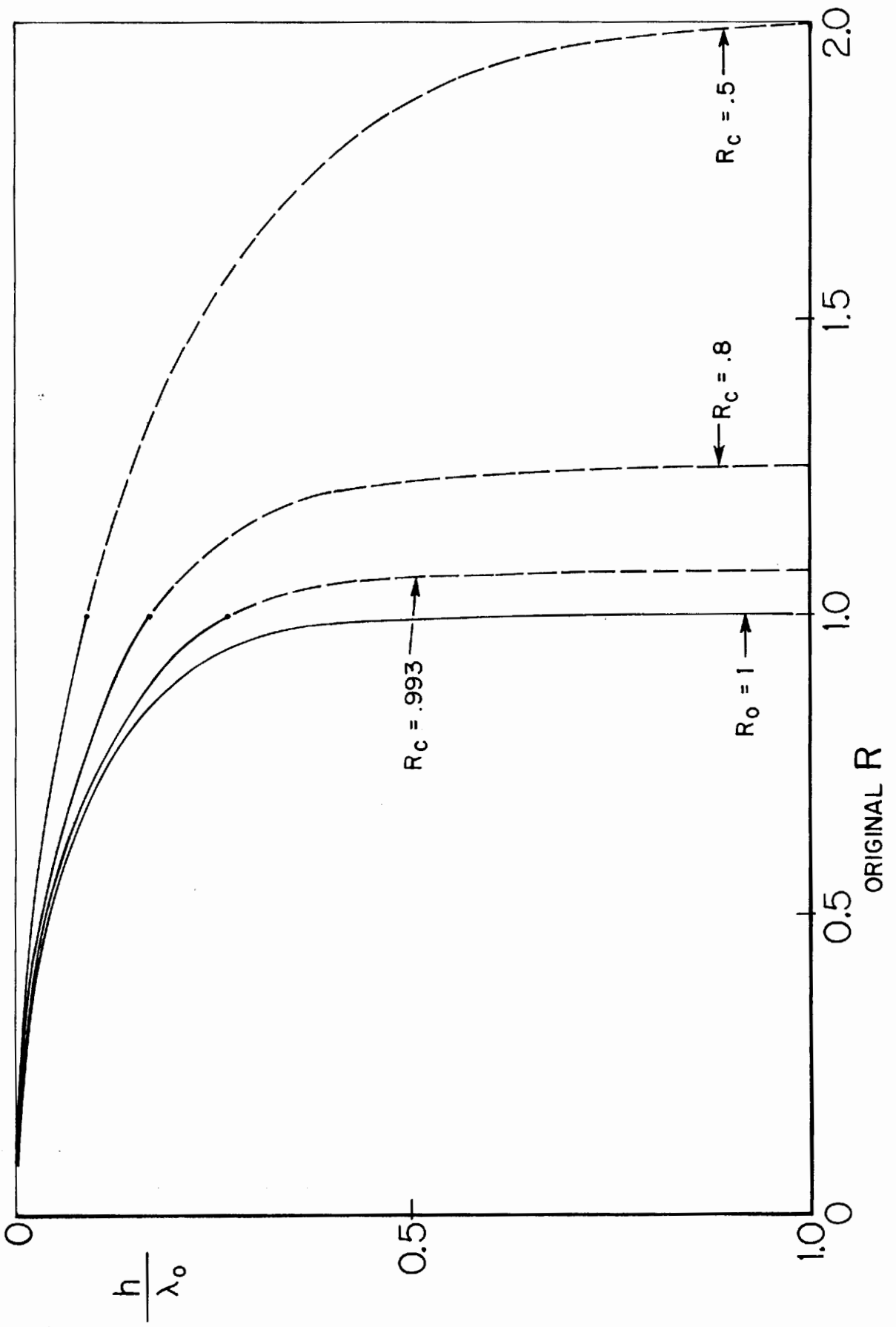
The peaks are now sparse due to the shift to
the right and the valleys have become very
deep.



30

CLIPPED ARTHUR'S ISLANDS NORMALIZED TO MAINTAIN
CONSTANT DIAMETER

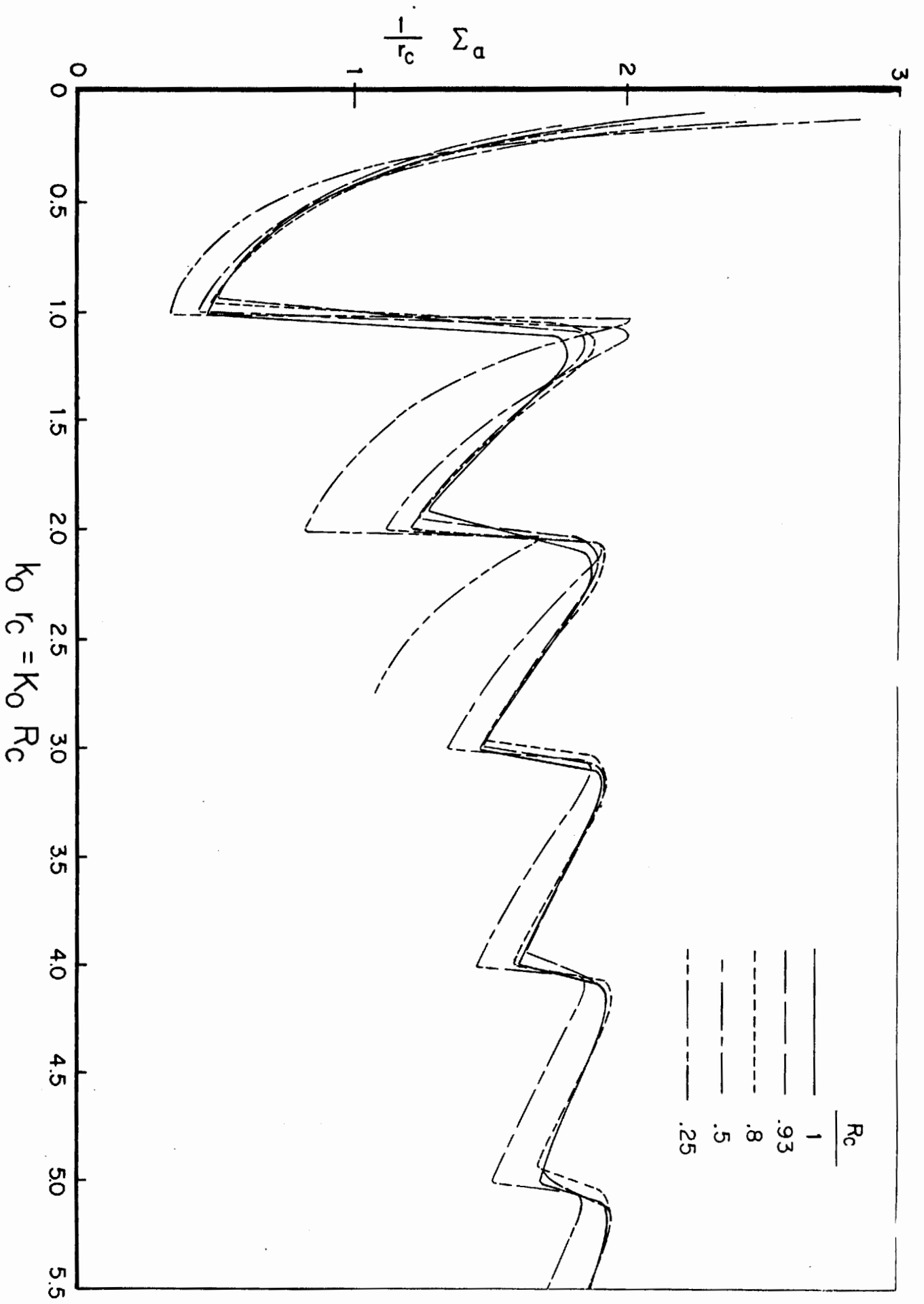
The radius r_0 may always be chosen to provide
a chosen outer radius and desired degree of
clipping.



31

ABSORPTION CROSS SECTION VS. $K_{oc} R_c$ FOR THE CLIPPED
ARTHUR'S ISLANDS OF FIGURE 30

For $R_c \geq 0.8$ the curves are nearly congruent.



6.0 RESPONSE OF ARTHUR'S ISLAND TO OFF-DESIGN WAVELENGTHS

6.1 The Phantom Island Method

All of the preceding analyses apply to any Arthur's Island designed for any wavelength λ_0 and of any chosen radius r_0 . The methods presented in the preceding sections predict the behavior of the island at its design wavelength λ_0 . One important question remains. Given any Arthur's Island designed for λ_0 , what is its response at any off design wavelength λ'_0 ? This information is essential in order to predict the response spectrum. The real ocean is seldom if ever monochromatic and wavelengths are constantly changing.

To meet these needs the method of "phantom islands" was evolved. Given any Arthur's Island designed at λ_0 and of radius r_0 , the response to impinging plane waves at any other wavelength λ'_0 is to be calculated. There exists an infinity of possible Arthur's Islands of design wavelength λ'_0 because any value of r'_0 may be chosen. Just one of these phantom islands having some particular radius r'_0 will have a shape which most closely approximates the shape of the original island. The predicted response of the phantom island at design wavelength λ'_0 is then taken to be the response of the original island at the off-design wavelength λ'_0 . This procedure is derived and delineated in the rest of this section. The two cases $\lambda'_0 < \lambda_0$ and $\lambda'_0 > \lambda_0$ differ slightly and are treated separately in some details.

6.2 The Shape of Arthur's Island

The shape of any circular atoll may be written as a function of local celerity

$$h = \frac{1}{k} C \operatorname{arctanh} C \quad (91)$$

For any Arthur's Island this becomes

$$h = \frac{\lambda_0}{2\pi} R \operatorname{arctanh} R \quad (92)$$

The shape of any other Arthur's Island of design wavelength λ'_0 is

$$h' = \frac{\lambda'_0}{2\pi} R' \operatorname{arctanh} R' \quad (93)$$

Set $r'_0 = \frac{r_0}{A}$ (94)

$$\lambda'_0 = \frac{\lambda_0}{B} \quad (95)$$

then

$$h' = \frac{\lambda_0}{2\pi} \frac{A}{B} R \operatorname{arctanh} AR \quad (96)$$

The factor B is determined by the choice of the off design wavelength λ'_0 . The task is then to determine the value of A which provides the best fit between h and h' in the most significant region. The procedure differs slightly for $\lambda'_0 < \lambda_0$ and $\lambda'_0 > \lambda_0$.

6.3 Best Fit In The Significant Region

Consider first the case of $\lambda'_0 < \lambda_0$. At some point R_N , the depth h equals $\frac{\lambda'_0}{2}$. Beyond this value of R, waves of wavelength λ'_0 no longer

sense the bottom and are not refracted, as is shown in Figure 7. Thus it would be counterproductive to enforce a curve fit between h' and h in the region $R_N < R \leq 1$. In this region, to a wave of wavelength λ'_0 the shape of the bottom is not relevant.

To establish R_N we equate h to $\frac{\lambda'_0}{2}$.

$$h = \frac{\lambda'_0}{2} = \frac{\lambda_0}{2\pi} R_N \operatorname{arctanh} R_N \quad (97)$$

$$R_N = \tanh \frac{\pi}{BR_N} \quad (98)$$

The significant region is then chosen to be

$$0 < R \leq R_N \quad (99)$$

The R.M.S. deviation between h' and h may be written

$$\Delta = \frac{\lambda_o}{2\pi} \left[\frac{1}{N} \sum_{n=1}^N (h_n - h'_n)^2 \right]^{\frac{1}{2}} \quad (100)$$

where

$$h'_n = \frac{\lambda_o}{2\pi} \frac{A}{B} R_n \operatorname{arctanh} A R_n \quad (101)$$

$$R_n = \frac{n}{N} R_N \quad (102)$$

and h_n is obtained by setting $A = B = 1$.

The minimum value of Δ , and hence the optimum value of A is obtained by a search procedure.

The relation between A and B found by this procedure is shown by solid circular points in Figure 32.

A minor modification to the procedure adapts it to use for $\lambda'_o > \lambda_o$. R_N is now chosen to be the point for which the depth of the original island becomes $\frac{\lambda_o}{2}$.

This means that R_N has a fixed value which is very near unity. In effect, the roles of h and h' have been interchanged in seeking the best curve fit. Thus for all $\lambda'_o > \lambda_o$ simply set R_N to the single value.

$$R_N = \tanh \frac{\pi}{R_N} = .996 \quad (103)$$

($R_N = .933$ was also tried, see Figure 32.)

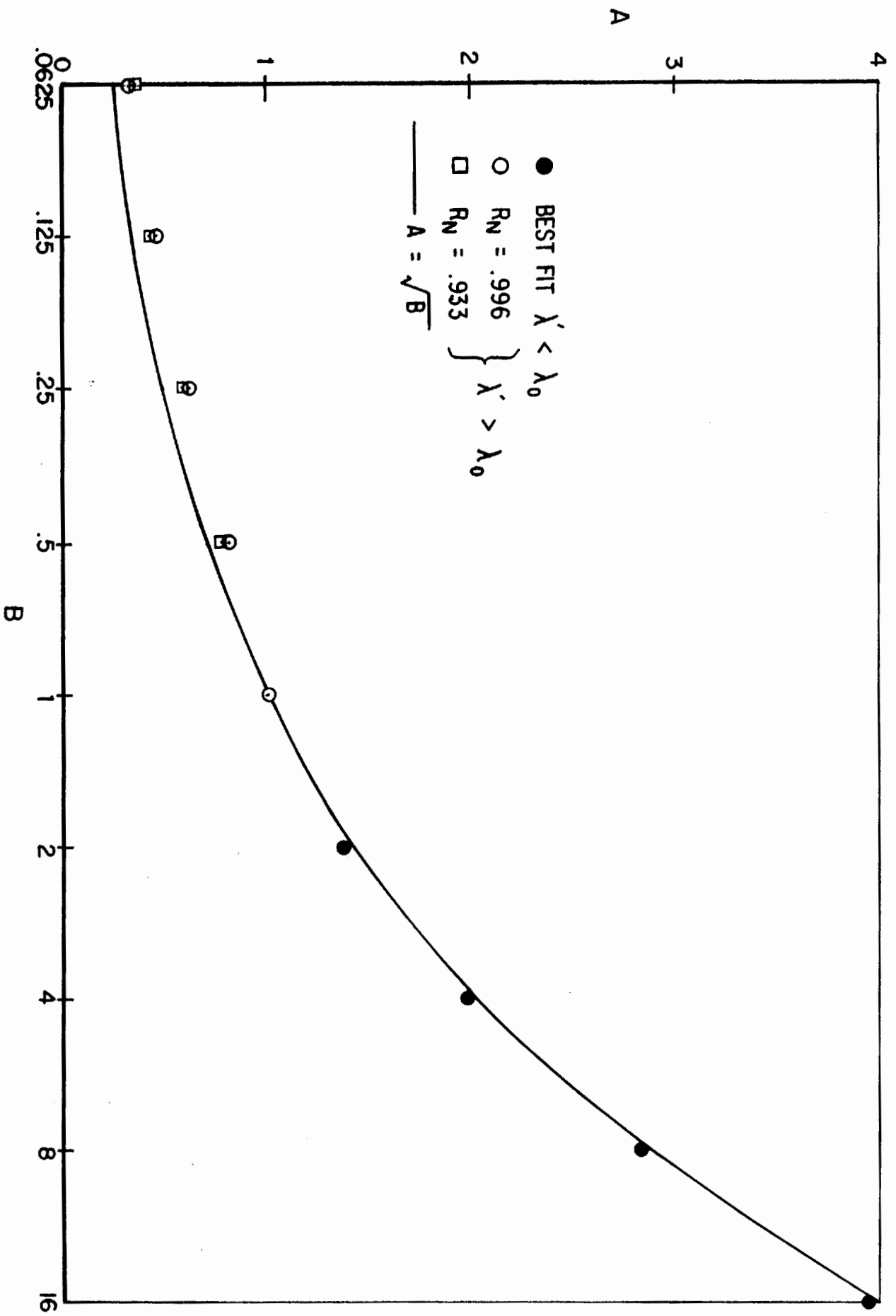
32

THE RELATION BETWEEN A AND B

The points represent A as a function of B that provide the best curve fit between Arthur's Island

and a phantom island for two selections of "significant region." The solid curve corresponds to

$$A = \sqrt{B}$$



The quality of the curve fits may be judged by comparing the minimum values of Δ to manufacturing tolerances. It appears that it might be difficult to construct an original island of design frequency λ'_0 and also its optimum phantom island of design frequency λ'_0 and then distinguish them by test at wavelength λ'_0 because of variations in their fabrication.

6.4 Relation of A to B

While drawing Figure 32 it was noticed that the values of A found by curve fitting were close to \sqrt{B} over the entire range of B as shown by the solid curve. The reasons for this were investigated as follows:

Each term $(h'_n - h_n)$ in equation 100 may be written,

$$\frac{\lambda'_0}{2\pi} (R_n \operatorname{arctanh} R_n - R_n \frac{A}{B} \operatorname{arctanh} A R_n). \quad (104)$$

The power series expansion for $\operatorname{arctanh} X$ is $X + \frac{X^3}{3} + \frac{X^5}{5} + +$

Thus

$$\begin{aligned} R_n & \left[R_n + \frac{R_n^3}{3} + \frac{R_n^5}{5} + \right. \\ & \left. - \frac{A}{B} \left(A R_n + \frac{A^3 R_n^3}{3} + \frac{A^5 R_n^5}{5} + + \right) \right] \\ & = R_n \left[R_n \left(1 - \frac{A^2}{B} \right) + \frac{R_n^3}{3} \left(1 - \frac{A^4}{B} \right) + + \right] \end{aligned} \quad (105)$$

This series tends to converge because R_n is always less than unity for every value of index n, thus the first term is quite dominant. This first term vanishes after setting $A = \sqrt{B}$.

If $A = \sqrt{B}$ the first term in the series becomes

$$\frac{R_n^4}{3} (1 - B) \quad (106)$$

The largest value of R_n is R_N which is less than unity. For $B < 1$ the term is small and for $B = 1$ becomes zero, as do all higher terms.

If $B > 1$ then as B increases R_N decreases rapidly as shown in equation 98.

Figure 32 compares the value $A = \sqrt{B}$ with values of A arrived at by minimizing the deviation Δ . Note that choosing R_N as .933 moves the best fit values of A closer to the curve $A = \sqrt{B}$ than did the choice $R_N = .996$. The latter corresponds to $h'_N = \frac{\lambda_o}{2}$ and the former to $\frac{\lambda_o}{4}$.

Setting $A = \sqrt{B}$ results in a major simplification in engineering calculations

$$B = \frac{\lambda_o'}{\lambda_o} = \frac{T'^2}{T^2} = \frac{f_o'^2}{f_o^2} \quad (107)$$

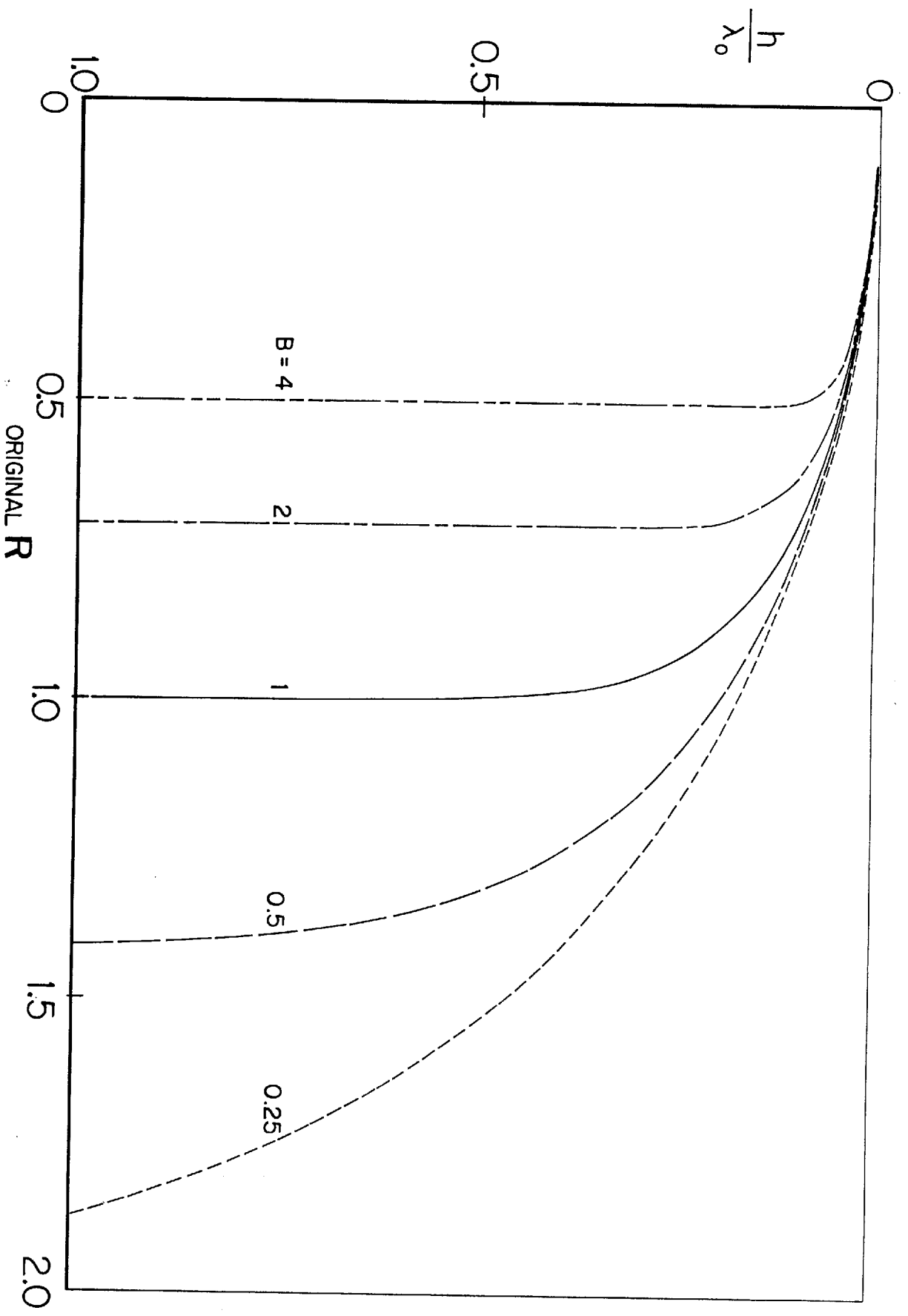
$$A = \frac{f_o'}{f_o} = \frac{r_o}{r_o'} \quad (108)$$

Thus the "best fit" phantom island is that for which r_o' is chosen as inversely proportional to its design frequency.

Figure 33 compares the shape of an Arthur's Island with two phantom islands of design wavelength $\lambda_o' = \frac{\lambda_o}{2}$ and $\lambda_o' = \frac{\lambda_o}{4}$. Figure 33 also compares the same Arthur's Island with two phantom islands with design wavelengths $\lambda_o' = 2 \lambda_o$ and $\lambda_o' = 4 \lambda_o$. The value $A = \sqrt{B}$ was used to construct these shapes.

THE SHAPE OF PHANTOM ISLANDS

These phantom island shapes are calculated
using $A = \sqrt{B}$



7.0 ABSORPTION CROSS SECTION SPECTRA

7.1 The Cross Sections of Phantom Islands

Referring to Figures 12, 13, and 14 the cross sections for the original Island are presented as functions of

$$K_o = k_o r_o = \frac{2\pi}{\lambda_o} r_o \quad (109)$$

The cross sections for any phantom island may be read by entering these same figures at

$$K_o' = \frac{2\pi}{\lambda_o'} r_o' = \frac{B}{A} K_o = \Delta K_o = \frac{f'}{f_o} K_o \quad (110)$$

The cross sections determined in this way apply to islands of radius r_o' . To compare cross sections to those of the original island the difference in radii should be compensated. To accomplish this, if $\lambda_o' < \lambda_o$ multiply the readoff normalized cross sections by

$$\frac{r_o'}{r_o} = \frac{1}{A} \quad (111)$$

If however $\lambda_o' > \lambda_o$ the multiplier is unity because r_o is the actual radius

7.2 Sample Spectra

Figure 34 presents absorption cross section spectra determined as described above, for three sizes of Arthur's Island, all designed for the same value of λ_o . K_o values are $\pi/2$, π , and 2π , corresponding to diameters of $\frac{\lambda_o}{2}$, λ_o , and $2\lambda_o$ respectively. The upper limit curve would be approached only by much larger islands. The rolloff for $\frac{f'}{f_o} > 1$ is due to the escape of the shorter wavelength rays.

The island for which $K_0 = \pi/2$ is clearly too small to be useful at long wavelengths. Its spectrum clearly shows the consequence of the deep valleys and sparse response peaks due to too few modes.

The island with $K_0 = \pi$ which is one design wavelength in diameter is probably close to optimum in most cases. Its low frequency response is much better than that of the island half its size and the deep valleys are absent.

The largest island, $K_0 = 2\pi$ shows continued improvement and approaches the upper limit curve. However it would require four times as much material to construct but would deliver only a little over twice the power. Thus it may lie beyond the point of diminishing returns in most cases.

These spectra were calculated for full depth Arthur's Islands ($h_0 = \infty$ at $R = 1$). They apply however to any clipped island so long as the clipping is not extreme, for example so long as $R_c > 0.8$.

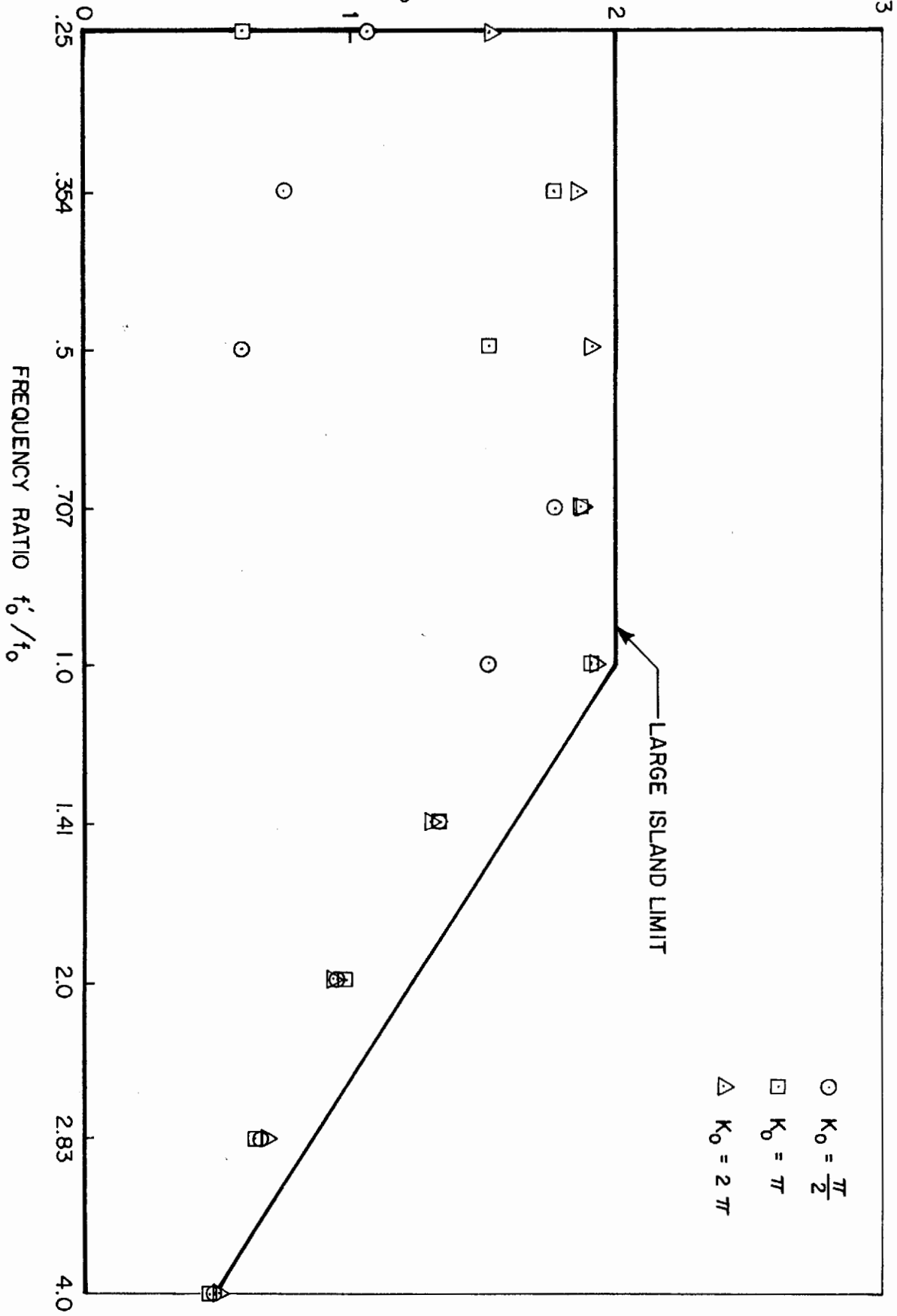
The final choice of design wavelength λ_0 should be based on long term wave energy spectra for a proposed site. The absorption spectral shape can then be matched to the available wave power spectrum to maximize yearly yield.

ABSORPTION CROSS SECTION SPECTRA

The rolloff for $f'_o/f_o > 1$ reflects the increasing percentage of escape paths. The undulations for $f'_o/f_o < 1$ result from mode sparsity for too small an island.

ADJUSTED ABSORPTION CROSS SECTION

(r_0 UNITS)



REFERENCES

- Abramowitz, M. and Stegun, I. A. 1964. "Handbook of Mathematical Functions With Formulas, Graphs, and Mathematical Tables," Dover Publications, Inc., New York.
- Arthur, R. S. 1946. "Refraction of Water Waves by Islands and Shoals With Circular Bottom Contours," Transactions American Geophysical Union, Vol. 27, No. II, Pages 168-177.
- Dwight, H. B. 1961, "Tables of Integrals and Other Mathematical Data," Macmillan, New York, page 255.
- George, J. 1979. "Calculation of Differential Cross Sections of Sound Geometrically Reflected From Impedance Cylinders," Journal of Acoustical Society of America, Vol. 65, No. 2, Pages 307-317.
- Morse, P. M. and Ingard, K. U. 1968. "Theoretical Acoustics," McGraw-Hill, New York, Pages 422-427.
- McCormick, M. E., 1981. "Ocean Wave Energy Conversion," Wiley, New York, Pages 124-129.
- Skudrzyk, E. 1971. "The Foundations of Acoustics," Springer-Verlag, New York, Pages 428, 278.
- Tyler, J. M., and Sofrin, T. G. 1961. "Axial Flow Compressor Noise Studies," Soc. Auto. Eng., 345D, Detroit.
- Wirt, L. S. 1979. "Wave Powered Motor," U.S. Patent, No. 4,152,895, May 8, 1979.